



HAL
open science

A geoelectric study of aquifers in the Essaouira coastal region, Morocco

Zakaria Ouzerbane, Tahar Aïfa, Abdellah El Hmaidi, Ali Essahlaoui,
Abdessamad Najine

► **To cite this version:**

Zakaria Ouzerbane, Tahar Aïfa, Abdellah El Hmaidi, Ali Essahlaoui, Abdessamad Najine. A geoelectric study of aquifers in the Essaouira coastal region, Morocco. *Journal of African Earth Sciences*, 2021, 183, pp.104309. 10.1016/j.jafrearsci.2021.104309 . insu-03268290

HAL Id: insu-03268290

<https://insu.hal.science/insu-03268290>

Submitted on 23 Jun 2021

HAL is a multi-disciplinary open access archive for the deposit and dissemination of scientific research documents, whether they are published or not. The documents may come from teaching and research institutions in France or abroad, or from public or private research centers.

L'archive ouverte pluridisciplinaire **HAL**, est destinée au dépôt et à la diffusion de documents scientifiques de niveau recherche, publiés ou non, émanant des établissements d'enseignement et de recherche français ou étrangers, des laboratoires publics ou privés.

Journal Pre-proof

A geoelectric study of aquifers in the Essaouira coastal region, Morocco

Zakaria Ouzerbane, Tahar Aïfa, Abdellah El Hmaidi, Ali Essahlaoui, Abdessamad Najine



PII: S1464-343X(21)00210-7

DOI: <https://doi.org/10.1016/j.jafrearsci.2021.104309>

Reference: AES 104309

To appear in: *Journal of African Earth Sciences*

Received Date: 22 March 2020

Revised Date: 24 May 2021

Accepted Date: 14 June 2021

Please cite this article as: Ouzerbane, Z., Aïfa, T., El Hmaidi, A., Essahlaoui, A., Najine, A., A geoelectric study of aquifers in the Essaouira coastal region, Morocco, *Journal of African Earth Sciences*, <https://doi.org/10.1016/j.jafrearsci.2021.104309>.

This is a PDF file of an article that has undergone enhancements after acceptance, such as the addition of a cover page and metadata, and formatting for readability, but it is not yet the definitive version of record. This version will undergo additional copyediting, typesetting and review before it is published in its final form, but we are providing this version to give early visibility of the article. Please note that, during the production process, errors may be discovered which could affect the content, and all legal disclaimers that apply to the journal pertain.

© 2021 Elsevier Ltd. All rights reserved.

A geoelectric study of aquifers in the Essaouira coastal region, Morocco

Zakaria Ouzerbane¹, Tahar Aïfa^{2,*}, Abdellah El Hmaïdi¹, Ali Essahlaoui¹, Abdessamad Najine³

¹ Water Science and Environmental Engineering, Department of Geology, Faculty of Sciences, Moulay Ismail University, BP 11201, Zitoune, Meknès, Morocco

² Univ Rennes, Géosciences Rennes - CNRS UMR6118, Bat.15, campus de Beaulieu, 35042 Rennes cedex, France

³ Department of Earth Sciences, Faculty of Science and Technology, Sultan Moulay Slimane University, BP 523 Mghila, 23000 Béni Mellal, Morocco

* Corresponding author: tahar.aifa@univ-rennes1.fr

A geoelectric study of aquifers in the Essaouira coastal region, Morocco

Zakaria Ouzerbane¹, Tahar Aifa^{2,*}, Abdellah El Hmaidi¹, Ali Essahlaoui¹, Abdessamad Najine³

¹ Water Science and Environmental Engineering, Department of Geology, Faculty of Sciences, Moulay Ismail University, BP 11201, Zitoune, Meknès, Morocco

² Univ Rennes, Géosciences Rennes - CNRS UMR6118, Bat.15, campus de Beaulieu, 35042 Rennes cedex, France

³ Department of Earth Sciences, Faculty of Science and Technology, Sultan Moulay Slimane University, BP 523 Mghila, 23000 Béni Mellal, Morocco

*Corresponding author: tahar.aifa@univ-rennes1.fr

Abstract

A geophysical study carried out in the framework of the water resources recognition within the Essaouira coastal area (Morocco) enabled to outline the spatial distribution of the Plio-Pleistocene and Cretaceous formations. It helped to determine the thickness and extension of the main aquifer used for irrigation purpose. The overall aim of this study is to highlight the hydrogeological structures of Essaouira Basin.

A total of 45 vertical electrical soundings (VES) were measured using linear Schlumberger array configuration with a maximum half-length (AB/2) of 1000 m along eight sections of 126 km total length. The number of soundings constituting the eight VES profiles depends on the topography and the obstacles encountered. The VES data were processed and interpreted. According to the thematic maps of the study area, the results indicate the existence of three types of VES with apparent resistivity values ranging from 44 to 320 Ω .m. In relationship with wells and mechanical drillings existing in the area, the analysis of the results obtained made it possible to derive from the quantitative and qualitative maps the different apparent resistivity variations of the aquifer and aquiclude geological layers.

The careful examination of these maps shows that the region around the Qsob River is of interest from a hydrogeological point of view. It is represented by a significant thick layer given the large extension of the resistive Plio-Pleistocene and Cretaceous formations. Geophysical studies show that this region is partially protected from marine intrusion given its location between Tidzi Diapir and hidden diapir from Essaouira which little plays the role of barrier. It is crossed by the Qsob River which lends itself as the main source of both these layers. The electrical discontinuities emerging from the superposition of the different maps,

38 E-W, NE-SW and NNE-SSW oriented, are abundant and dense in the north Haha region
39 (Qsob River). Generally, the salt water circulates along these discontinuities from West to
40 North and Northeast which explains the abundance of low apparent resistivity values recorded
41 northeastwards. This geophysical reconnaissance is the most important for water supply of
42 this area affected by increasingly long periods of drought.

43 **Keywords:** Essaouira Basin; Qsob River; Plio-Pleistocene; Cretaceous; groundwater; vertical
44 electrical sounding; apparent resistivity.

45

46 **1. Introduction**

47 The shortage of Morocco's water supplies is not an unusual concept, it stems from the
48 peculiarities of the region's geographical and climatic context. The availability of this
49 resource in quantity and quality will be compounded by many processes (e.g., Calow et al.,
50 2010; Manu et al., 2016). It should be noted that the unconscious rise over the years has had a
51 negative effect on the appearance and scale of arid and semi-arid areas of marine and waste
52 water. Furthermore, in essence, the presence/expansion of saline waters has an opposite effect
53 on groundwater supplies and agricultural areas that have become polluted with water and
54 waterlogged areas (Urish and Frohlich, 1990; Sherif et al., 2006; Attwa and Zamzam, 2020).

55 This will accentuate the tension between supply and demand in relation to climate change.

56 The impact of these changes by 2020, will result in a decrease in renewable water resources of
57 4,5 billion m³/year and 3 billion m³/year for mobilizable resources divided into 2,4 billion
58 m³/year of surface resources and 0.6 billion m³/year of groundwater (Sinan et al., 2009). This
59 decrease automatically influences the water/inhabitant capital, which will be 682
60 m³/inhabitant/year by 2020 instead of 775 m³/inhabitant/year in the absence of climate
61 change. By 2050, the decline in the country's water resources will most probably be between
62 15% and 20% and should bring the water/inhabitant capital probably to modules of about 500
63 m³/year/inhabitant (Sinan et al., 2009). Due to its geographical location, Morocco is subject to
64 various climatic influences varying from north to south under the effect of latitude and from
65 west to east under the effect of the continentality. Precipitation is characterized by significant
66 irregularity that is expressed in one year, even more pronounced south of the Atlas range from
67 one year to another. The countries of the Mediterranean region, including Morocco, have
68 experienced endured periods of drought over the past two decades. However, the issue of
69 overexploitation of groundwater resources continues, despite the efforts of governments
70 (Chafouq et al., 2018). As a consequence, Essaouira Basin is marked by a high density of
71 wells leading to overexploitation of aquifers.

72 The study area is represented by the coastal area of Essaouira Basin, which is part of the
73 Moroccan Atlantic coastline. It is a space that is given a heavy responsibility in the socio-
74 economic development of the country. This development implies a significant increase of the
75 water needs in the upcoming years as well for the drinking water supply as for the irrigation
76 and industry. The Essaouira Basin has experienced, like the other regions of Morocco, a
77 significant decline in water intake in both quantity and quality. This situation has led to the
78 reduction of agricultural productivity and the degradation of several ecosystems. However,
79 this basin has an aquifer system consisting of a set of uneven aquifers that can offer a natural
80 regulating capacity making them valuable to ensure a safe and steady supply. The reserve also
81 enables temporary overexploitation to meet seasonal needs to the degree that replenishment
82 becomes possible. The diffuse pollution generated by marine waters has been amplified by
83 point sources of pollution mainly represented by human and agro-industrial activities
84 (Karroum et al., 2017). As a result, salt levels recorded in some places far exceed the drinking
85 water or irrigation standard (Bahir et al., 2001). This situation may eventually jeopardize the
86 sustainability of agricultural activity as a whole, undermine public health and compromise the
87 self-purification power of groundwater. These waters flow slowly through the subsoil, so that
88 contamination from human activities will persist for long periods for certain individual
89 aquifers ranging from a few years to several decades or more. In other words, in coastal areas,
90 groundwater resources require special attention to minimize saltwater intrusions, either
91 locally or at a regional scale (Chamchati et al., 2013). The extension of the saltwater intrusion
92 depends on the geometry, the structure and properties of the aquifer, the stresses applied to
93 the aquifer (pumping, etc.) and the flow of freshwater and salty exchanging with the
94 surrounding environment (Ouzerbane et al., 2014; Bahir et al., 2019). This situation is more
95 important because groundwater is the only accessible water supply for local communities in
96 this study area.

97 Geophysical study, hydrogeological mapping and hydrogeochemical analysis, as well as the
98 compilation of agricultural and socio-economic data are all data that must be integrated in
99 digital form so as to obtain easily land classification maps used by forest managers, planners
100 and plan for the proper implementation of groundwater drilling. The use of a geographic
101 information system (GIS) is of tremendous importance in this regard. Focus has been
102 provided to the detailed explanation of the area's regional and local geological context. All the
103 lithological, petrographic, sedimentological and structural details of all current formations
104 have been obtained by geological reconnaissance (Souid, 1983; Medina, 1994; Piqué, 1994;
105 Broughton and Trépanier, 1993; Piqué and Laville, 1996 ; Piqué et al., 1998 ; Hafid, 2000;

106 Mader et al., 2017). These data enable the facies and levels likely to be obtained by
107 underground water tables to be defined, as well as to favor the selection of the geophysical
108 methods best suited to the study context and to better enforce the geophysical measurement
109 grids. The resistivity method has been chosen, since it is suitable for monitoring soil horizons
110 within basins as well as aquifer reservoirs (Eluwole et al., 2018). It can thus be applied
111 successfully to Essaouira Basin coastline. This method has also been applied to a wide range
112 of fields and reported in numerous papers from the literature (e.g., Bhattacharya and Patra,
113 1968 ; Bose and Ramkrishna, 1978; Urish and Frohlich, 1990; Devi et al., 2001; Sainato et
114 al., 2003; Owen et al., 2005; Sharma and Baranwal, 2005; Singh et al., 2005; Yadav and
115 Singh, 2007; Francese et al. 2009; Kumar et al., 2010, 2014; Chandra et al., 2012; Ebraheem
116 et al., 2012; Zaidi and Kassem, 2012; Anechana et al., 2015; Manu et al., 2016; Sikah et al.,
117 2016). As a non-destruction method to the environment, it provides useful subsurface
118 information and also gives a contrast between rock layers having different electrical
119 properties (Store et al., 2000; Okrah et al., 2012). Aside from groundwater prospecting, the
120 Vertical Electrical Resistivity (VES) method, among other techniques, is applied in (i)
121 mineral and petroleum exploration (Fon et al., 2012; Fuh et al., 2019; Mashhad et al., 2020),
122 (ii) agricultural groundwater identification in semi-arid regions (Asfahani, 2016; Bersi and
123 Saibi, 2020) (iii) landslide modelling (Perrone et al., 2004; Sajinkumar et al., 2015), (iv)
124 saltwater intrusion investigation (Sherif et al., 2006), (v) environmental pollution (Ogungbe et
125 al., 2012) and (vi) foundation engineering (Akintorinwa and Abiola, 2011 ; Arisona et al.,
126 2020), etc. The VES data, which can be interpreted using curve matching technique through
127 various algorithms (Dey and Morrison, 1979; Zhody, 1989; Gupta et al., 1997 ; Yadav et al.,
128 1997 ; Basokur, 1999 ; Singh et al., 2005, 2013 ; Piatti et al., 2010 ; Srinivas et al., 2012), is
129 well useful for estimating the aquifer properties and the subsurface geology (Flathe, 1955;
130 Ghosh, 1971; Kosinky and Kelly, 1981; Mazac et al., 1985; Yadav and Abolfazli, 1998;
131 Asfahani, 2016 ; El Bouhaddioui et al., 2016).

132

133 **2. Geological framework**

134 Essaouira synclinal study area is generally a low, especially near Essaouira; it is part of the
135 coastal area of the basin with surface of 1418 km². It is limited to the north by Jbeb Hadid, to
136 the south by Tidzi River, to the east by the reliefs of Chiadma and Haha and by the Tidzi slide
137 and to the west by the Atlantic Ocean. It is not very hilly and is characterized by low hills
138 with altitudes between 0 and 800 m, modelled by a low-density hydrographic network that

139 flows into the Atlantic Ocean (Ouzerbane et al., 2018). From north to south, two units can be
140 distinguished namely the south Chiadma Unit and the north Haha Unit (Fig. 1).

141 The geological formations flush in the synclinal zone of Essaouira are generally of
142 Quaternary and Plio-Pleistocene age (Fig. 2). From the south to the north of the study area,
143 the stratigraphic series extends from the Triassic to the Quaternary (Ouzerbane, 2015;
144 Ouzerbane et al., 2019; Cohen et al., 2020). They are outcropping in the southeastern part of
145 the study area in the Tidzi region in a NE-SW direction forming the Tidzi diapir over a large
146 area while in the extreme south of the study area, these formations outcrop on a smaller area
147 along Aghbalou River. Saliferous red clays, dolerites/basalts and reddish sandstone pelites are
148 mainly known in these formations.

149 **2a. Main geological formations**

150 The Upper Jurassic geological formations age mainly consist of gypsiferous and marly
151 limestones. They outcrop at the level of Jbel Hadid north of the Essaouira Syncline. Whereas,
152 the Cretaceous formations outcrop on the entire Essaouira Basin with thicknesses varying
153 from one place to another. They are exposed to the east by gray marls and lumachellic
154 limestones of Santonian age, turquoise limestone dolomitic limestones, limestones, marls and
155 gypsiferous marls, Cenomanian in age, along Oued Tidzi. To the west, the outcrops of Albian
156 formations correspond to green marls on top of which Maastrichtian dolomitic limestones
157 outcrop. The Lower Cretaceous formations are also exposed to the northwest of the study
158 area.

159 The Plio-Pleistocene and Quaternary formations constitute the main outcrops in the study
160 area. From the center of the area to the Atlantic coast westwards, the sand dunes and
161 calcarenites become important in terms of distribution and thickness. The Plio-Pleistocene
162 formations are outcropping almost over the entire area by sandstones, fine sands, yellow
163 limestones and conglomerates.

164 **2b. Hydrogeological context**

165 In the study region, for the daily consumption of the inhabitants, groundwater remains the key
166 water supplies that provide drinking water supply, industrial and domestic needs, and less
167 essential irrigation downstream of the Qsob River. The combination of the impact of tectonics
168 and diapirism has contributed to the division of the basin into many aquifer systems that are
169 poorly understood in their activity and hydraulic relationships. The value of the aquifer
170 system varies from the north to the south of the region according to the existence of the
171 geological formations that comprise the reservoir and its extension. The Cretaceous plateau
172 multi-layer aquifer and the Plio-Pleistocene aquifer formed on the coastal strip are the main

173 aquifers in the basin. On the other hand, the Jurassic aquifer, which is located deeper in the
174 center of the study area, is less important. The different aquifers in the area are hydraulically
175 interconnected and interdependent and thus constitute a single hydraulic system.

176 *Plio-Pleistocene aquifer*

177 The Plio-Pleistocene formation in the study area is a matrix reservoir consisting of sandstone
178 dunes and shell limestones. It extends along the Atlantic coast on a strip of 20 km wide and
179 30 km long.

180 According to mechanical soundings and reconnaissance wells carried out in the area by the
181 Tenssift Hydraulic Basin Agency, the reservoir is productive only when it is in perched
182 position resting on the impervious Cretaceous or Jurassic marls. The Plio-Pleistocene
183 formations rest directly on the permeable formations. The water infiltrates vertically to feed
184 the deep aquifer. The aquifer's saturated thickness ranges between 10 and 60 m and the
185 extracted flow rate does not exceed 10 l/s (Mennani, 2001).

186 On the one side, the groundwater feeding is carried out by the infiltration of the rainwater and
187 on the other side by the infiltration along the rivers, with a general flow of the aquifer to the
188 ocean due to the Cretaceous formations dipping to the west (Ouhamdouch et al., 2018). The
189 reservoir has a transmissivity with a large dispersion: it varies from 6×10^{-2} to 4.5×10^{-5} m²/s,
190 under the effect of feeding the groundwater by the waters of the Qsob River.

191 *Cretaceous aquifer*

192 It is the most important aquifer due to its extension and its hydrodynamic characteristics. Its
193 properties are related to the existence of discontinuities represented by stratification plans,
194 giving rise to sources, by fracturing and also by the creation of karstification phenomenon.

195 It includes (i) the Santonian yellow dolomitic and dolomitic limestones whose thickness may
196 reach 100 m, cracked and karstified Turonian limestones with a thickness of 40 to 80 m, the
197 Cenomanian lumachellic limestones and gray marly limestones with gypseous traces,
198 fractured fossiliferous limestones and Barremian-Aptian sandstones. Often, these different
199 Cretaceous reservoirs contain free aquifers sometimes captive. In the absence of a significant
200 impervious layer between the different levels gives it the character of a multilayer system,
201 where the Turonian aquifer is the most essential with a transmissivity varying from 2×10^{-4} to
202 9×10^{-3} m²/s. The Cretaceous reservoir is fed mainly by rains and along the Igrounzar River to
203 the south of Meskala and downstream to the south of Essaouira and possibly from the
204 overlying Plio-Pleistocene aquifer (Mennani, 2001). The aquifer is drained by springs
205 emerging along the Rivers Igrounzar and Qsob. The general flow of the aquifer is towards the
206 north and the northwest before reaching the Atlantic Ocean

207

208 **3. Geoelectrical prospecting**

209 During this initial process, the geophysical research performed in the Essaouira coastal region
210 started with the geological identification of the land to be prospected. This recognition was to
211 obtain all the details relating to the characteristics of the soil and subsoil. Indeed, the
212 geological study made it possible to better identify the type of rock or material, the structure
213 of the different formations, the sedimentological environment, the mode of formation or
214 genesis of the different facies and also to identify the state of alteration and fracturing. This
215 collected geological information helped to establish correlations with the hydrological,
216 lithological and petrographic information (Hodlur et al., 2006). It also facilitates the choice of
217 the most adapted measurement devices to the study context and to better implement the data
218 acquisition profiles. In parallel with this study phase, all data relating to the hydrogeology of
219 this area were collected. In fact, they were collected by means of piezometric surveys and
220 lithological identification of aquifer levels.

221 Subsequently, a program of geoelectric data acquisition campaigns during the years 2011,
222 2012 and 2013, involved the implementation of 45 vertical electrical soundings (Fig. 3), using
223 a Schlumberger type device, totaling 126 km in length. The acquisition of the data was
224 followed by the establishment of geoelectric sections on which are indicated the layers with
225 their resistivities, thicknesses and depths.

226 The equipment used for vertical electrical soundings (VES) is a Syscal R1 Plus
227 resistivitymeter specially designed for surface and underground prospecting. It is perfectly
228 adapted to hydrogeological and structural studies. It also allows to study the resistivity
229 variations as a function of depth (VES) as well as lateral resistivity variations along a profile
230 (electrical profiling). The Syscal R1 resistivity meter is designed to work with different types
231 of devices such as Schlumberger, Wenner, dipole-dipole, pole-dipole, and pole-pole (Sharma,
232 1997).

233 The profiles of the vertical electrical soundings were oriented in such a way as to: (i) cross
234 orthogonally the faults and folded structures assumed to play a role in the flows (vector and/or
235 buffer seat); (ii) capture the maximum of the stratigraphic series in order to test the hydraulic
236 behavior of the main formations (aquifer, aquitard, impervious, roof, wall, etc.) and to have as
237 much information as possible on their geometry; (iii) 'touch' the anomalous structures,
238 especially the one due to the rise of diapirs; (iv) crossing the 'frontier' sectors hoping to
239 intercept the main 'conduits' of underground water if the hypothesis of dominance of the

240 preferential flows is confirmed, otherwise, invalidate or qualify such an assumption if
241 necessary.

242 The method of interpreting the results obtained by geoelectric techniques is based on the use
243 of charts, mainly during data acquisition in the field, but with the development of computer
244 tools, the geophysicists use efficient computer programs. In this case, IPI2WIN software was
245 used (Geoscan-M Ltd., 2001). The latter interprets the data starting from a user-proposed
246 initial model. It makes it possible to elaborate models of the subsoil by bringing the
247 experimental curves closer to theoretical curves according to an iterative process.

248 In order to obtain a result consistent with the data gathered in the field, the number of layers,
249 their thicknesses and their resistivities are modified each time (Table 1). Since several
250 solutions are possible, based on the geological data of the area, the model is subject to certain
251 limits and the model that gives the best appearance of these two curves is used for the
252 Essaouira electrical sounding interpretation (e.g., Redouani et al., 2013). The interpretation of
253 the data obtained from the acquisition in the coastal zone, correlated and calibrated by the
254 mechanical drilling carried out by the Tenssift Hydraulic Basin Agency, made it possible to
255 synthesize the development of each layer, variations in thickness and/or resistivity and
256 highlight the anomalies that might affect them (Table 2).

257

258 **4. Results**

259 Geoelectrical prospecting by vertical electrical soundings (VES) is a geophysical method that,
260 applied in hydrogeology, will provide information on the geometry of potential reservoirs,
261 their lithological nature and the spatial evolution of these characteristics. The interpretation of
262 the VES results, carried out in the Essaouira coastal zone, correlated and calibrated by
263 soundings and mechanical drillings carried out by the Tenssift Hydraulic Basin Agency,
264 helped to make a synthesis on the development of each layer by computing its thickness
265 and/or resistivity variations to best fit the registered anomalies.

266 ***4a. Description of vertical electrical soundings***

267 The limitation and resolution of VES models decreases with the probleme of equivalence or
268 ambiguity, depth, thin layers of low resistivity contrasts cannot be detected . This implies that
269 many models correspond to the same set of VES data (Himi et al., 2017; Essahlaoui et al.,
270 2003; Wafiq et al., 2019). Depending on the shape of the VES curves realized and the
271 succession of the conductive and resistant levels, one can distinguish three types:

272 **Type A:** For this family, the sounding curve representing the evolution of the apparent
273 resistivity as a function of the half-length $AB/2$ of the measuring device has a "bottom-of-

274 boat" shape which translates, first of all, into a decrease values of the apparent resistivity
 275 followed by a slight increase thereof. This type of electric sounding pattern is that of a three-
 276 layer basement model corresponding to the superimposition of two strong terrains separated
 277 by a comparatively conductive third, often ending in a conductive layer (Fig. 4a). Indeed, as
 278 the device's size grows, the current pumped into the subsoil enters deeper and deeper
 279 structures.

280 In the same way, apparent resistivity values increase as current lines reach the deep resistor.
 281 Hence, the observed shape of the sounding curve. This family is represented by the VES
 282 curves at sites 2-4, 10, 25, 27-29, 31, 38-39, 43-45, 47 and 52.

283 The data collected in these electrical holes led to identical survey curves (Fig. 3). Their
 284 interpretation has practically led to a top-down terrain model by the following entities:

285 - A relatively resistant ground R_0 intrinsic resistivity that can reach 367 $\Omega.m$ (site 31). This
 286 land probably corresponds to the conglomeratic and alluvial level, and to Plio-Pleistocene
 287 sand.

288 - A conductive C_1/C_2 level of resistivity lower than 100 $\Omega.m$ (site 29) corresponding to the
 289 Santonian or Albian marls, which represent, on the one hand, the impervious basement of the
 290 Plio-Pleistocene aquifer and the roof of the Turonian or Barremian-Aptian water table, on the
 291 other hand.

292 The resistivity of the alluvial complex hardly exceeds 200 $\Omega.m$ and its thickness is variable.
 293 Generally, it has a prismatic shape, thick in the center of the basin and thin away from the
 294 Qsob River. This complex is home to a groundwater that plays an important role in the socio-
 295 economic life of the local population.

296 - A resistant R_1/R_2 whose resistivity can reach 480 $\Omega.m$ (site 38). This level, corresponding to
 297 marly limestones and limestones attributed to the Turonian or to massive limestones and
 298 sandstone of the Vraconian, represent the largest underground aquifer of the Essaouira Basin.

299 Depending on the location of the electrical sounding, a second conductive level C_2 can be
 300 reached below the resistant level R_2 , attributed to the Cenomanian marls and marly limestones
 301 or to the Barremian-Aptian marls. It can be seen that this first VES family (Type A) reveals a
 302 typical subsoil structure consisting of an alternation of three, four or sometimes five
 303 electrically differentiated terrains.

304 **Type B:** For this family, the sounding curve representing the evolution of the apparent
 305 resistivity as a function of the half-length $AB/2$ of the measuring device has a "bell" shape
 306 which results, first of all, in an increase in the apparent resistivity values followed by a
 307 decrease (Fig. 4b). The current injected into the basement reaches formations deeper and

308 deeper. It circulates at the beginning of the sounding exclusively in the superficial conductor,
 309 which allows low values. Then, when it reaches the resistant intermediate ground, the values
 310 gradually increase as more and more volume of it contributes to the measurement. In the same
 311 way, the apparent resistivity values decrease when the current lines reach the deep conductor.
 312 Hence, the observed shape of the sounding curve. This family is represented by the VES
 313 curves at sites 12, 17-19, 21, 23-24, 22, 30, 33, 35-37, 42, 48-49, 51, 53-55 and 57.

314 The data collected at the level of these electrical soundings led to survey curves (Fig. 3), the
 315 interpretation of which led practically to a top-down terrain model by the following entities:

316 - A highly conductive ground C_0 intrinsic resistivity that can reach $20 \Omega.m$ and variable
 317 thickness. This land corresponds to the superficial alluvial cover very abundant in the region,
 318 clay or topsoil of Quaternary and/or Plio-Pleistocene age.

319 - A resistant level R_0 or R_1 according to the local geology, it corresponds either to a Plio-
 320 Pleistocene sandstone level of small thickness and significant resistivity or to a significant
 321 level of massive Turonian or Barremian-Aptian limestones covered by recent formations. The
 322 apparent (true) resistivity sometimes exceeds $1300 \Omega.m$ if the surface layers are dry.

323 - A C_1 deep conductor ($16 \Omega.m$) responsible for the final decrease of the curve. It is a marly
 324 layer, which constitutes the impermeable substratum of the R_0 or R_1 aquifer.

325 **Type C:** Electrical soundings of this type represent the evolution of the resistivity as a
 326 function of the half-length $AB/2$ of the measuring device, presented by curves having a
 327 "descending staircase" shape which results in a continuous decrease in resistivity (Fig. 4c).
 328 Indeed, as and when the increase in the size of the device, the current injected into the
 329 basement reaches formations deeper and deeper. It circulates at the beginning of the hole
 330 exclusively in the surface resistant, which allows important values. Then, when it reaches the
 331 intermediate conductive ground, the values gradually decrease as a more and more important
 332 volume of it contributes to the measurement. In the same way, the apparent resistivity values
 333 decrease when the current lines reach the deep conductor. Hence, the observed shape of the
 334 sounding curve. A small number of VES at sites 6, 11, 13, 15, 40-41, 46, 50 and 56 represents
 335 this family.

336 The data collected at the level of these electrical soundings led to survey curves (Fig. 3), the
 337 interpretation of which led practically to a top-down terrain model by the following entities:

338 - A very resistant surface ground of intrinsic resistivity R_0 , which can exceed $200 \Omega.m$, and of
 339 variable thickness. This terrain corresponds to the very abundant Plio-Pleistocene sandy or
 340 sandstone overburden or to the resistant Cretaceous R_1 .

341 - A moderately resistant level R_1/R_2 , according to the local geology, probably corresponds to
 342 Cretaceous marly limestones.

343 - A deep conductive layer C_2 (16 $\Omega.m$) responsible for the final decline of the curve. It is a
 344 very important marly layer which constitutes the impervious substratum of aquifers in the
 345 region and may correspond to Santonian, Cenomanian or Albian marls.

346 ***4b. Geoelectrical section***

347 From the quantitative interpretation of the VES data correlated with the borehole data, several
 348 geoelectric sections have been drawn. These sections, generally E-W oriented, clearly show
 349 the heterogeneity of the geological facies. The fairly complex geological structure of the
 350 region and the vertical and horizontal relationships between the various hydrogeological
 351 aquifers help to target the resistant formations which can be important aquifers taking into
 352 account their physical and geometric characteristics (Essahlaoui et al., 2001). In this article,
 353 we will only present a single geoelectric section located north of the sector (Fig. 5). This
 354 geoelectric section is carried out from the VES at sites 15, 28 to 31 and 33 (Fig. 5). It shows
 355 the following lithological variations:

356 ***Quaternary and Plio-Pleistocene formations***

357 This section shows a conductive layer correlated with clays and topsoil eastwards. Thicker
 358 than previous sections, with a 15 m thickness, it shows a resistivity ranging from 25 to 45
 359 $\Omega.m$. westwards, the thickness of the resistant layer R_0 becomes important and varies between
 360 12 and 80 m with a resistivity ranging from 132 to 1300 $\Omega.m$. The resistant level R_0 is
 361 correlated with the very resistant Plio-Pleistocene sandstones (data from Mechanical drilling
 362 1489/43) (Fig. 5).

363 ***Cretaceous formation***

364 It is divided into three important levels. One notice that the conductive level C_1 is only found
 365 in the eastern part, detected by the SEV at site 28. It disappears going westwards from site 29
 366 where the series presents from top to bottom:

367 - A Resistant layer R_1 , characterized by a thickness of 40 to 56 m with a resistivity oscillating
 368 from 63 to 90 $\Omega.m$. It is correlated with Cenomanian marly limestones.

369 - The C_2 conductive layer is well represented in this section by its thickness of 56 to 60 m
 370 (sites 29 and 31) and with a resistivity varying from 36 to 44 $\Omega.m$. It is correlated with the
 371 Cenomanian plastic gray marls.

372 - A resistant layer R_2 of high resistivity, varying from 105 to 195 $\Omega.m$, whose roof is affected
 373 by soundings 29 and 31 (Fig. 5). The correlation with drilling 1489/43 shows that it
 374 corresponds to the massive Uppermost Albian (Vraconian) limestones.

375 One still notice the presence of a subsidence of the electric levels towards the west, the rise of
376 these levels can be explained by the Hadid-Kourati faulting system (Ouzerbane et al., 2013).

377 ***4c. Qualitative Interpretation of the vertical electrical soundings***

378 The results of the geoelectrical analysis carried out in the Essaouira coastal zone resulted in
379 the production of several maps of apparent resistivity. Ideas and information on the lateral
380 resistivity variations of a given area for different subsurface layers, corresponding to different
381 spacings of the electrical current injection electrodes AB, can be obtained from these
382 qualitative maps.

383 ***Apparent resistivity map***

384 The establishment of the apparent resistivity map for the selected line length (AB=160 m)
385 allows the characterization of the outcrop or subsurface deposits (Fig. 6). The analysis of this
386 map shows a lateral variation of the resistivity, with conductive zones located in the east
387 (Ounara-Had Draa Region) and in the center between Qsob River and Tidzi River.

388 The impacts of the subsurface become insignificant when increasing the current injection line
389 AB. Analysis of the apparent resistivity map indicates resistivity development in the study
390 region from the south to the northwest. Similarly, the apparent resistivity values measured,
391 from northeast to west, range from 46 to 135 Ω .m. This resistivity increase is due to the
392 deepening of the Cretaceous resistive formations, from northwest to south and from west to
393 northeast. Such deepening becomes essential in the south of Qsob River (Fig. 7).

394 ***4d. Quantitative Interpretation of the vertical electrical soundings***

395 A series of quantitative maps was drawn up from the analysis of the mechanical drilling and
396 the quantitative results of the electrical soundings in order to evaluate the thicknesses of the
397 various Plio-Pleistocene and Cretaceous electrical levels and their lateral extensions (Fig. 8).

398 ***Isopach maps***

399 For the evaluation of the different electrical levels of the Plio-Pleistocene and Cretaceous
400 formations, three maps have been established. They respectively give: (i) the thickness and
401 the lateral extension of the superficial Plio-Pleistocene formations; (ii) the spatial distribution
402 of impervious and semi-impermeable Cretaceous formations; and (iii) the distribution of
403 permeable aquifer formations attributed to Cretaceous limestones and marly limestones,
404 which form a multilayer system in the Essaouira Basin.

405 ***Isopach map of the Plio-Pleistocene aquifer***

406 A steady rise in thickness from east to west of the study region is revealed by the isopach map
407 analysis of Plio-Pleistocene surface formations. With maximum values of the order of 100 m

408 observed generally in the west, precisely on the coastal road of Essaouira-Safi, the minimum
409 values are observed in the northeast of the study area at the regional level (Fig. 9).

410 ***Isopach map of the Cretaceous resistant layers***

411 The examination of the isopach map of the Cretaceous resistant obtained shows a thickening
412 of the limestones from north to south (Fig. 10). The maximum is reached in the Qsob River
413 where the Turonian and Cenomanian resistant layers may exceed 150 m in thickness, forming
414 hence a captive aquifer in this eastern area, fed by rainwater and runoff from Qsob River
415 (Fekri, 1993).

416 Thickness is also crucial in the Tidzi region where Santonian marly limestones and Turonian
417 karstified limestones are covered directly by the Plio-Pleistocene formations. Towards the
418 south, in Smimou region, the less thick resistant layer corresponds to Barremian-Aptian
419 limestones and flint limestones formed beneath the Plio-Pleistocene formations.

420 ***Isopach map of the Cretaceous conductive layers***

421 The isopach values shown on this map correspond to the difference between the wall depth of
422 the Plio-Pleistocene aquifer and that of the Cretaceous aquifer roof. The analysis of the
423 conductive levels, resulting from the interpretation of the electrical soundings and of the
424 correlations between the logs of the mechanical drillings, led us to determine in each position
425 of electric sounding, the thickness of the conductive Cretaceous layers which may correspond
426 to gray and plastic marls and marly limestone formations (Fig. 11).

427 ***Isobath map of Cretaceous resistant roof***

428 The isobath map corresponds to the depth of the resistant roof attributed to the Cretaceous.
429 This map gives the spatial distribution of the depth of the resistant, which forms the deepest
430 and most important aquifer in the area, varying from 0 to more than 1500 m. The analysis of
431 this map shows that the area around Qsob River presents the location where the resistant
432 aquifer is very deep, with an increase from east to west, compared to the whole studied area
433 (Fig. 12).

434 ***4e. Interaction of marine water and groundwater in the coastal area***

435 Geophysical studies show that the synclinal of Essaouira, which is crossed by Qsob River, is
436 located between two diapirs. The hidden diapir of Essaouira contains, by its position along the
437 coastal zone, a natural barrier which can play the role of protecting groundwater against
438 marine water intrusion.

439 Generally, electrical conductivity gives an idea of the mineralization of groundwater,
440 therefore provides information on its salinity and allows its quality to be assessed. The first
441 interpretations of the map established by measurements of electrical conductivity (Fig. 14),

442 carried out during surveys of water points (wells and sources, Table 3), show a spatial variety
443 of values along a single direction NE-SW. The minimum values of the order of 1334 $\mu\text{S}/\text{cm}$
444 (wells W25 and W56) are recorded in the center of the area and towards the southeast at the
445 level of the axis of wells W25 and W65 (Fig. 14). Going to the S-W and N-E of the study
446 area, the values increase to reach maximum values around 6524 $\mu\text{S}/\text{cm}$ (e.g., well W34).

447 The waters of the Plio-Pleistocene reservoir have a varied electrical conductivity going from
448 the center of the study area where the values are minimum (1334 $\mu\text{S}/\text{cm}$) and maximum (6524
449 $\mu\text{S}/\text{cm}$) eastward and northwestward, respectively. The very high values of electrical
450 conductivity are recorded in the N-W far from the Atlantic coast, which explains why the
451 salinity of the water is very likely in direct relation with the marly and gypsum formations.
452 On the other hand, the Cretaceous aquifer system is formed by an assembly of raised and
453 sagging blocks separated by faults. These are organized according to three major directions
454 (NNE-SSW, NNW-SSE and E-W), which are found on a regional scale. They can play the
455 role of partial communication and/or barrier between marine water and groundwater. The
456 impact of marine intrusion is localized in the region of Essaouira and has no influence at the
457 regional scale according to several studies which have been developed for the private
458 investment sector (Ouzerbane, 2015; Ouzerbane et al., 2018; Ouhamdouch et al., 2018, 2021;
459 Bahir et al., 2019).

460 Recent studies on the origin of the salinization of the Plio-Pleistocene and Turonian aquifers
461 have been addressed, namely by Ouhamdouch et al. (2021) who used hydrogeochemical and
462 isotopic approaches: the couples (Na, Cl), (Ca, Mg), (Br, Cl), ($\delta^2\text{H}$, $\delta^{18}\text{O}$), ($\delta^{18}\text{O}$, Cl). The
463 intersection of all these results approaches is consistent with a weak marine intrusion
464 influence located at Cap Sim. The calculated maximum mixing rate at the borehole 11/51
465 (seawater/freshwater) is of the order of 16%. The remaining boreholes analyzed by
466 Ouhamdouch et al. (2021) display molar ratios different from that of sea water, indicating that
467 the salinization of the study area is outside the phenomenon of marine intrusion and therefore
468 the existence of another source of salinization (dissolution of salts).

469

470 **5. Discussion**

471 Geoelectrical prospecting by vertical electrical soundings (VES) is a geophysical method that,
472 applied in hydrogeology, will provide information on the geometry of possible reservoirs,
473 their lithological nature and the spatial evolution of their characteristics (e.g., Atzemoglou and
474 Tsourlos, 2012). The interpretation of the VES results, carried out in the coastal zone of the
475 Essaouira Basin, correlated and calibrated by the soundings and mechanical drillings carried

476 out by the Tensift Hydraulic Basin Agency, made it possible to get a synthesis on the
477 behavior of each layer, its thickness and/or resistivity variations and the corresponding
478 anomaly detected. The interpretation of a vertical electrical survey consists in determining the
479 real resistivities and the thicknesses of the different terrains. It is visible from a diagram in bi-
480 logarithmic coordinates representing the apparent resistivities as a function of the half-length
481 ($AB/2$) values of the measuring device. This interpretation is based on the hypothesis of the
482 horizontality of the formations surveyed, but in nature this case is not always valid, one
483 therefore admits values of dip of the order of 15° to 20° (Essahlaoui, 2000; Essahlaoui et al.,
484 2001, Essahlaoui and El Ouali, 2003).

485 In the analysis of the results obtained by geoelectric methods, the graphical approach has
486 always been useful. In the present study, the IPI2WIN software was used for modelling
487 (Geoscan-M Ltd., 2001) through least-squares approximation using an iterative processing to
488 fit both the experimental and theoretical curves and get the best model. To better change the
489 shape of both curves, the user has the possibility to modify the model.

490 The results of the geoelectrical study carried out in the Essaouira coastal zone, led to the
491 establishment of some maps of apparent resistivity. A set of six maps were computed: (i) two
492 apparent resistivity maps with a device measurement for $AB=160$ (Fig. 6) and $AB=500$ (Fig.
493 7), (ii) three isopach maps for the Plio-Pleistocene aquifer (Fig. 9), the Cretaceous resistant
494 (Fig. 10) and conductive (Fig. 11) formations, and (iii) an isobath map for the Cretaceous
495 resistant roof (Fig. 12). One notice that the apparent resistivity maps for $AB=160$ m (500 m)
496 may characterize shallow (deep) deposits. These qualitative maps have been established to
497 evaluate the lateral resistivity variations which could be related to lithology variations,
498 moisture content, clay content and salinity (Alfaifi et al., 2019).

499 Analysis of the apparent resistivity map for $AB=160$ m (Fig. 6) shows a lateral variation in
500 resistivity, with conductive zones located east of the study area (Ounara-Souk Had Draa
501 region) and in the center between Qsob River and Tidzi River. These conductive zones may
502 correspond to Cretaceous marls and marly limestones with a resistivity ranging between 44
503 and $77 \Omega.m$. Whereas, the Plio-Pleistocene outcrops are very small, resistant zones with
504 resistivities larger than $77 \Omega.m$, covering the majority of the area with maximum values
505 around $320 \Omega.m$ in the northwest, especially in the north of Qsob River. In correlation with
506 mechanical drilling and geological maps, these zones can be correlated with sandstones,
507 Quaternary and Plio-Pleistocene sand and alluvium, except south of Tidzi River. In fact, the
508 distribution of the apparent resistivity values (using $AB=160$ m), south of Tidzi River, may
509 correspond to Barremian-Aptian flint limestones and marly limestones ($98-120 \Omega.m$).

510 When increasing the current injection line AB, the effects of the subsurface become
511 negligible. Examination of the apparent resistivity map obtained for AB=500 m shows a
512 resistivity growth from south to northwest. Similarly, from northeast to west, the apparent
513 resistivity values measured vary from 46 to 135 Ω .m. Such an increase is due to the
514 deepening of the Cretaceous resistant formations, from northwest to southwest towards the
515 northeast. It becomes important south of Qsob River (Figs. 7, 10). According to the analysis
516 of the apparent resistivity map (using AB=500 m), a resistant zone stands out to the northwest
517 and corresponds to the Cretaceous marly limestones and limestones. With apparent resistivity
518 values varying from 81 to 135 Ω .m, the maximum resistivity is recorded in the northwest at
519 sites 15-21 and 33, but also in the east at site 45. This resistant zone separates two conductive
520 zones located northeast and south (south of Qsob River), with resistivities ranging from 46 to
521 67 Ω .m, corresponding to the Cretaceous marls and marly limestones .

522 Concerning the quantitative interpretation of the results, the analysis of the isopach map, the
523 Plio-Pleistocene surface formations (Fig. 9) shows a gradual increase in thickness going from
524 east to west. Maximum values of the order of 100 m are observed generally westwards,
525 mainly on the coastal road of Essaouira-Safi, whereas minimum values are observed in the
526 northeast at the regional scale. In fact, within the area of Ounara and Souk Had Draa a
527 thickness of 8 to 30 m is recorded, and south of the Qsob River where the thickness of the
528 Plio-Pleistocene formations varies from 30 to 40 m with sometimes values higher than 40 m
529 along the river. Comparison of this isopach map (Fig. 9) with that of the apparent resistivity
530 (using AB=160 m) (Fig. 6), shows that the thick zones correspond to electric horizons of high
531 resistivity values with good spatial continuity. These are areas attributed lithologically to
532 sandstones and sands which form the important aquifer of the region. The superposition of
533 this map with the map of the piezometric level of the region also allows to determine the
534 thickness of the wet aquifers.

535 The values shown on the isopach map of the resistant and permeable Cretaceous level (Fig.
536 10) correspond to the difference between the wall of the Plio-Pleistocene aquifer formations
537 (C_1) in areas where both resistants R_0 and R_1 are in contact. The second wall of the
538 Cretaceous conductive roof (C_2) in the areas where the thickness of the resistant layer is low
539 corresponds to the difference between the side of the conductive wall C_1 and the conductive
540 roof of the Cretaceous C_2 . The interpretation of the various electrical soundings and the
541 correlations with the drillings and the mechanical soundings existing in the region make it
542 possible to determine at each position of VES the thickness of the Cretaceous resistant layer.
543 This layer is also important in the Tidzi region (mechanical sounding 365/51 and VES at site

544 54). Southwards, within the Smimou region, the less thick resistant layer corresponds to
545 Barremian-Aptian limestones and flint limestones developed beneath the Plio-Pleistocene
546 formations. In the north, the isopach map shows a thickness between 85 to 110 m of the
547 Cenomanian resistant layer corresponding to limestones and marly limestones. It developed
548 between two conductive Cenomanian and Barremian-Albian layers, namely C_1 and C_2 ,
549 respectively. Towards the extreme north of the area, the resistant to a thickness of 32 to 84 m
550 and corresponds very likely to massive Vraconian limestones.

551 Examination of the isopach map of the conductive formations (Fig. 11) shows a gradual
552 thickening of Santonian gray marl from southeast to northwest in the region delimited by
553 Qsob and Tidzi Rivers. Their maximum thicknesses can be observed south of Qsob River,
554 where the marly layer may exceed 150 m thick (VES at sites 41-42). It is corroborated by the
555 lithology within the drilling well 362/51. This marly layer forms a good impermeable layer
556 for both the important Quaternary and Turonian reservoirs of the region. At the northeast, in
557 the Ounara-Souk Had Draa region, there is a gradual thickening of the Cenomanian marls and
558 marly limestones that are outcropping in the eastern part of the area, where it becomes very
559 thick. In its northern part the thickness of the conductive layer becomes low to zero,
560 especially east of Essaouira-Safi road and south of Ounara village. The comparison of the
561 isopach map (Fig. 11) obtained with that of the apparent resistivity with a length of $AB=500$
562 m (Fig. 7), indicates a similarity between the distribution of the apparent resistivity of the
563 electrical levels prospected and the variation of their thickness. It is noted that the marls and
564 marly limestones conducting levels having resistivities lower than $70 \Omega.m$ in the map of the
565 apparent resistivity with $AB=500$ m, coincide with the zones where the thickness of the
566 conducting levels is very important. The resistant zones with values greater than $70 \Omega.m$
567 coincide with zones where the thickness is small or zero.

568 From a hydrogeological point of view, the conductive layers represent the wall of the Plio-
569 Pleistocene aquifer and the roof of the Cretaceous aquifer. The decrease or the absence of
570 their thickness in the study area lead to a draining phenomenon where the Plio-Pleistocene
571 resistant rests directly on the Cretaceous resistant, corroborating hence the presence of sterile
572 hydrogeological boreholes. The significant thickness of the marly layer in the northeast zone
573 (Ounara-Souk Had Draa) and between Qsob River and Tidzi River represents an important
574 wall for the Plio-Pleistocene aquifer. This explains the abundance and overexploitation of this
575 groundwater by the inhabitants for drinking water and irrigation needs.

576 The analysis of the isobath map, corresponding to the depth of the Cretaceous resistant roof,
577 demonstrates that the area around Qsob River represents the location where the resistant

578 aquifer is very deep, increasing westwards (Fig. 12). It is noted that in the north the low
579 values observed indicate that the resistant is shallower or superficial. north of Tidzi River, the
580 resistant layer has not detected using a device length of $AB=1000$ m. where gray marls and
581 marly limestones, have very large thicknesses, are outcropping all along the Tidzi River. One
582 may also note a set of discontinuities that can be the result of normal faulting affecting these
583 formations and accommodating grabens. These are generally due to the rise of Tidzi diapir in
584 the east and the Essaouira hidden diapir in the west (Taj-Eddin, 1991), where the Upper
585 Cretaceous (Cenomanian-Turonian) formations are into abnormal contact with the Lower
586 Cretaceous (Barremian-Albian) formations.

587 In practice, the isobath map obtained constitutes a document of primordial interest and with
588 the maps of the hydrodynamic parameters of the groundwater (permeability K , transmissivity
589 T and degree of storage S) they are necessary for the implantation of exploitation boreholes.
590 The different maps computed, whether qualitative or quantitative, are complementary to the
591 geoelectric sections. The assembly of these resistivity models provides an overview of the
592 resistivity variation in the E-W and N-S directions across the geophysical measurement area.
593 Remember that the electrical sounding profiles were positioned above the drilling and
594 mechanical soundings and hydrogeological wells to help explain the structure of the deep
595 subsoil in these locations. Given the strong resistivity contrast between sandstones, sands,
596 limestones, marls and clays, the demonstration of such structures would have been obvious.
597 Compared to the western portion, the structure of the region is thus broken into fragments of
598 anticlines and synclines of reduced scale. The positioning of diapirs of unequal size favored
599 this discontinuous and wrinkled structure (Fig. 13).

600

601 **6. Conclusions**

602 The geoelectrical study carried out in the framework of the reconnaissance of the water
603 resources in the Essaouira coastal zone enabled us to (i) determine the spatial distribution of
604 the Plio-Pleistocene and Cretaceous formations and (ii) emerge from the quantitative and
605 qualitative maps, the different variations of apparent resistivity of the geological layers
606 constituting the aquifers and aquicludes.

607 The comparison of all the acquired data made it possible to have an overall view of the
608 variation of the resistivity in the E-W and N-S directions across the area covered by the
609 measurements. The profiles were placed in relation to the hydrogeological wells in order to
610 better clarify the subsurface structures at these locations. Given the strong contrast of
611 resistivity between sandstones, limestones, marls and clays, the nature of these structures has

612 been highlighted. The sandstone masses appear clearly on the maps and are materialized on
613 the ground by dominant reliefs, separated from the overlying terrain by NE-SW regional
614 faults. Compared to the western portion, the structure of the region is thus broken into
615 fragments of anticlines and synclines of reduced scale. This discontinuous and wrinkled
616 structure favored the emplacement of diapirs of unequal importance. Towards the north, it is
617 noted that the fragmented structures gave way to more monotonous stratigraphic forms. It
618 thus appears that the Essaouira Basin suggests itself as a vast synclinal zone open on the ocean.
619 This area is affected by several folds and accidents that allow the individualization of many
620 synclines. The combination of the impact of the Atlasic tectonics and diapirism has resulted in
621 a sequence of anticlines and synclines. The entire basin is fractured from the Hercynian
622 tectonics process by large events that stretch under the cover and are inherited.

623 The Upper Cretaceous reservoir is by far the most important aquifer due to its extension and
624 hydrodynamic characteristics. It is a multilayer system that includes the Santonian dolomitic
625 and dolomite limestones, the cracked and karstified limestones of the Turonian, and the
626 Cenomanian limestones and marly limestones. Its aquifer properties are related to the
627 existence of discontinuities within these formations. Such discontinuities are represented by
628 the S_0 stratification planes (which sometimes give rise to sources), by fracturing (parallel to
629 the S_0 planes) and also by the development of karstification phenomena. An assembly of
630 raised and collapsed blocks separated by faults constitutes the Cretaceous aquifer system.
631 They are organized according to three major directions (NNE-SSW, NNW-SSE and E-W),
632 which are found at the regional scale and which correspond to the reactivation of the deep
633 faults of the Hercynian basement. These faults can play a role of drain or main axis of water
634 flow of the aquifer within this aquifer system, since they may constitute impermeable barriers
635 and thus prevent any flow occurrence. Following this configuration in blocks of the aquifer,
636 the hydrodynamic flow of the layer is discontinuous. There may be hydrodynamic
637 interconnections between adjacent blocks, particularly with regard to these conducting faults.
638 Systematic monitoring of the quality and quantity of groundwater (water resources and
639 reserves) is necessary to avoid deterioration and scarcity of water to ensure water supply.

640 Finally, the study of different maps obtained shows that the area around Qsob River is of
641 great interest from a hydrogeological point of view. It is represented by a very important layer
642 given the wide extension of the Plio-Pleistocene and Cretaceous resistant formations with
643 very large thicknesses. It is crossed by the Qsob River which presents these two layers as the
644 main source of recharge.

645

646 **Acknowledgements**

647 We are greatly indebted to the NATO for their financial support through program CLG
 648 n°983954 and for granting part of this study. The logistic support during exploration and
 649 sampling was funded by the Faculty of Science and Technology, Sultan Moulay Slimane
 650 University - Béni Mellal (Morocco). We are also grateful to anonymous reviewers for the
 651 fruitful remarks that helped to improve the manuscript. This is a contribution of the
 652 UNESCO-IGCP638 program.

653

654 **Table captions**

655 **Table 1.** Vertical electrical sounding at site 28 and its interpretation model (type A) computed
 656 using IPI2WIN software (Geoscan-M Ltd., 2001). VES: Vertical Electrical Sounding; X, Y,
 657 Z: UMT coordinates and elevation (m); ρ : resistivity, H : height, D : depth; black and red
 658 curves relate to experimental and theoretical models, respectively; blue line: approximation
 659 of both models.

660 **Table 2.** Interpretation of electrical soundings with the range of resistivity, the number of
 661 layers and their thickness.

662 **Table 3.** Data of measurements of the electrical conductivity of well waters of the Plio-
 663 Pleistocene aquifer. WH: Well height, T: temperature, PL: Piezometric level, EC: Electrical
 664 conductivity at 25°C.

665

666 **Figure captions**

667 **Fig. 1.** Geographic location and Digital Elevation Model (DEM) of the study area (Projected
 668 on the WGS84 system).

669 **Fig. 2.** Geological map showing the main formations of the Essaouira coastal zone
 670 (Ouzerbane, 2015; Ouzerbane et al., 2019).

671 **Fig. 3.** Location of vertical electrical soundings (VES) and the mechanical drillings (MD) in
 672 the study area. Dashed line: VES cross-section, square: VES, triangle: MD.

673 **Fig. 4.** Vertical electrical sounding showing three possible layers: (a) *type A*, a conductive
 674 layer between two resistive layers, (b) *type B*, a resistive layer between two conductive
 675 ones, (c) *type C*, two resistive layers upon a conductive one, respectively. ρ_a : apparent
 676 resistivity ($\Omega.m$), R_0 , R_1 , R_2 : resistant layers; C_1 , C_2 : conductive layers. $AB/2$ (m): half-
 677 length profile.

678 **Fig. 5.** Geoelectrical section located at the north of the study area (see Fig. 3) in correlation
 679 with mechanical drilling 1489/43.

680 **Fig. 6.** Apparent resistivity map for AB=160 m.

681 **Fig. 7.** Apparent resistivity map for AB=500 m.

682 **Fig. 8.** Example of correlation and wedging between VES at site 53 and mechanical drilling
683 363/51 (final depth at 152 m), in agreement with two conductive layers (sandy marls and
684 marly limestones) on top of a resistant one (limestone) (Ouzerbane, 2015).

685 **Fig. 9.** Isopach map of the Plio-Pleistocene aquifer.

686 **Fig. 10.** Isopach map of Cretaceous resistant formations.

687 **Fig. 11.** Isopach map of Cretaceous conductive formations.

688 **Fig. 12.** Isobath map of the Cretaceous resistant roof.

689 **Fig. 13.** Jurassic roof isobath map and diapir intrusions of the Essaouira coastal zone
690 (modified, from Duffaud, 1963).

691 **Fig. 14.** Map of electrical conductivity of the Plio-Pleistocene reservoir (Ouzerbane, 2015).

692

693 **References**

- 694 Akintorinwa, O.J., Abiola, O., 2011. Subsoil evaluation for pre-foundation study using
695 geophysical and geotechnical approach. *Journal of Emerging Trends in Engineering and*
696 *Applied Sciences*, 2(5), 858-863.
- 697 Alfaifi, H., Kahal, A., Albassam, A., Ibrahim, E., Abdelrahman, K., Zaidi, F., Alhumidan, S.,
698 2019. Integrated geophysical and hydrochemical investigations for seawater intrusion: a
699 case study in southwestern Saudi Arabia. *Arabian Journal of Geosciences*, 12:372.
700 <https://doi.org/10.1007/s12517-019-4540-8>
- 701 Anechana, R., Noye, R.M., Menyeh, A., Manu, E., Okrah, C., 2015. Electromagnetic and
702 vertical electrical sounding for groundwater potential Assessment of Kintampo North
703 Municipality of Ghana. *Journal of Environmental Earth Sciences*, ISSN 2224-3216 (paper)
704 ISSN 225-0948 5(12)
- 705 Arisona, A., Ishola, K.S., Nawawi, M.N.M., 2020. Subsurface void mapping using
706 geophysical and geotechnical techniques with uncertainties estimation: case study of Kinta
707 Valley, Perak, Malaysia. *Springer Nature, Applied Sciences*, 2:1171.
708 <https://doi.org/10.1007/s42452-020-2967-x>
- 709 Asfahani, J., 2016. Hydraulic parameters estimation by using an approach based on vertical
710 electrical soundings (VES) in the semi-arid Khanasser valley region, Syria. *Journal of*
711 *African Earth Sciences*, 117, 196–206. <https://doi.org/10.1016/j.jafrearsci.2016.01.018>
- 712 Attwa, M., Zamzam, S., 2019. An integrated approach of GIS and geoelectrical techniques for
713 wastewater leakage investigations: Active constraint balancing and genetic algorithms

- 714 application, *Journal of Applied Geophysics*, 175, 103992.
 715 <https://doi.org/10.1016/j.jappgeo.2020.103992>
- 716 Atzemoglou, A., Sourlos, P.T., 2012. 2D interpretation of vertical electrical soundings:
 717 application to the Sarantaporon basin (Thessaly, Greece). *Journal of Geophysics and*
 718 *Engineering*, 9, 50–59. doi:10.1088/1742-2132/9/1/006
- 719 Bahir, M., Jalal, M., Mennani, A., 2001. Pollution nitraté des eaux souterraines du bassin
 720 synclinal d'Essaouira. *Journal of Environmental Hydrology*, 18(9), 1-9.
- 721 Bahir, M., Ouazar, D., Ouhamdouch, S., 2019. Dam effect on groundwater characteristics
 722 from area under semi-arid climate: case of the Zerrar dam within Essaouira basin
 723 (Morocco). *Carbonates and Evaporites*, 34(3), 709-720. [https://doi.org/10.1007/s13146-](https://doi.org/10.1007/s13146-019-00497-0)
 724 [019-00497-0](https://doi.org/10.1007/s13146-019-00497-0)
- 725 Bose, R.N., Ramkrishna, TS., 1978. Electrical resistivity surveys for ground water in the
 726 Deccan trap country of Sangli district, Maharashtra. *Journal of Hydrology*, 38, 209–221.
- 727 Basokur, A.T., 1999. Automated 1D interpretation of resistivity soundings by simultaneous
 728 use of the direct and iterative methods. *Geophysical Prospecting*, 47, 149–177.
- 729 Bersi, M., Saibi, H., 2020. Groundwater potential zones identification using geoelectrical
 730 sounding and remote sensing in Wadi Touil plain, Northwestern Algeria. *Journal of*
 731 *African Earth Sciences*, 172, 104014. <https://doi.org/10.1016/j.jafrearsci.2020.104014>
- 732 Bhattacharya, P.K., Patra, H.P., 1968. Direct current geoelectric sounding: principles and
 733 interpretation. *Elsevier Science Publishing Co., Inc., Amsterdam*, 144p.
- 734 Broughton, P., Trépanier, P., 1993. Hydrocarbon generation in the Essaouira Basin of western
 735 Morocco. *A.A.P.G. Bulletin*, 77(6), 999-1015.
- 736 Calow, R.C., Macdonald, A.M., Nicol, A.L., Robins, N.S., 2010. Ground water security and
 737 drought in Africa: linking availability, access, and demand. *Ground Water*, 48, 246-256.
 738 <https://doi.org/10.1111/j.1745-6584.2009.00558.x>
- 739 Chafouq, D., El Mandour, A., El Gettafi, M., Himi, M., Chouikri, I., Casas, A., 2018.
 740 Hydrochemical and isotopic characterization of groundwater in the Ghis-Nekor plain
 741 (Northern Morocco). *Journal of African Earth Sciences*, 139, 1-13.
 742 <https://doi.org/10.1016/j.jafrearsci.2017.11.007>
- 743 Chamchati, H., Bahir, M., 2013. Potential hydrogeological, environment and vulnerability to
 744 pollution of the Plio-Quaternary aquifers of the coastal basin of Essaouira (Morocco).
 745 *Journal of Environmental Earth Sciences*, 3(10), 170-185.
- 746 Chandra, S., Nagaiah, E., Reddy, D.V., Ananda Rao, V., Ahmed, S., 2012. Exploring deep
 747 potential aquifer in water scarce crystalline rocks. *J. Earth Syst. Sci.*, 121(6):1455–1468

- 748 Cohen, K.M., Finney, S.C., Gibbard, P.L., Fan, J.-X., 2020. The ICS International
 749 Chronostratigraphic Chart. *Episodes*, 36, 199-204.
 750 <http://www.stratigraphy.org/ICSchart/ChronostratChart2020-03.pdf>
- 751 Devi, S.P., Srinivasulu, S., Raju, K.K., 2001. Delineation of groundwater potential zones and
 752 electrical resistivity studies for groundwater exploration. *Environmental Geology*,
 753 40,1252–1264.
- 754 Dey, A., Morrison, H., 1979. Resistivity modelling for arbitrarily shaped two-dimensional
 755 structures. *Geophysical Prospecting*, 27, 106-136. [https://doi.org/10.1111/j.1365-
 756 2478.1979.tb00961.x](https://doi.org/10.1111/j.1365-2478.1979.tb00961.x)
- 757 Duffaud, F., 1963. Bassin du Sud-Ouest marocain, cartes d'isopaques des séries Jurassiques,
 758 Crétacés et Tertiaires. *Société Chérifienne du Pétrole*, Département Exploration, Rabat,
 759 Morocco.
- 760 Ebraheem, A.M., Sherif, M.M., Al Mulla, M.M., Akram, S.F., Shetty, A.V., 2012. A
 761 geoelectrical and hydrogeological study for the assessment of groundwater resources in
 762 WadiBih, UAE. *Environmental Earth Sciences*, 67(3),845–857.
- 763 El Bouhaddioui, M., Mridekh, A., Kili, M., El Mansouri, B., El Gasmi, E., Magrane, B., 2016.
 764 Electrical and well log study of the Plio-Quaternary deposits of the southern part of the
 765 Rharb Basin, northern Morocco. *Journal of African Earth Sciences*, 123, 110-122.
- 766 Eluwole, A.B., Olorunfemi, M.O., Ademilu, O.L., 2018. Soil horizon mapping and textural
 767 classification using micro soil electrical resistivity measurements: case study from Ado-
 768 Ekiti, southwestern Nigeria. *Arabian Journal of Geosciences*, 11 :315.
 769 <https://doi.org/10.1007/s12517-018-3652-x>
- 770 Essahlaoui, A., 2000. Contribution à la reconnaissance des formations aquifères dans le bassin
 771 de Meknès-Fès (Maroc). Prospection géo-électrique, étude hydrogéologique et inventaire
 772 des ressources en eau. *Thèse de Doctorat*, Ecole Mohamadia des Ingénieurs, Rabat,
 773 Morocco, 258p.
- 774 Essahlaoui, A., Sahbi, H., Bahi, L., El Yamine, N., 2001. Preliminary survey of the structure
 775 and hydrogeology of the western Saiss Basin, Morocco, using electrical resistivity. *Journal
 776 of African Earth Sciences*, 32(4), 777-789. [https://doi.org/10.1016/S0899-5362\(02\)00054-4](https://doi.org/10.1016/S0899-5362(02)00054-4)
- 777 Essahlaoui, A., El Ouali, A., 2003. Détermination de la structure géologique de la partie Sud
 778 de la plaine du Saiss (bassin de Meknès-Fès, Maroc) par la méthode géoélectrique. *Bulletin
 779 of Engineering Geology and Environment*, 62, 155–166. [https://doi.org/10.1007/s10064-
 780 002-0178-x](https://doi.org/10.1007/s10064-002-0178-x)

- 781 Fekri, A., 1993. Contribution à l'étude hydrogéologique et hydrogéochimique de la zone
782 synclinale d'Essaouira (Bassin synclinal d'Essaouira). *Thèse 3ème cycle*, Marrakech, 172p.
- 783 Flathe, H., 1955. Possibilities and limitations in applying geoelectrical methods to
784 hydrogeological problems in the coastal areas of North West Germany. *Geophysical*
785 *Prospecting*, 3, 95–110.
- 786 Fon, A.N., Che, V.B., Cheo, E.S., 2012. Application of electrical resistivity and chargeability
787 data on a GIS platform in delineating auriferous structures in deeply weathered lateritic
788 terrain, Eastern Cameroun. *International Journal of Geosciences*, 3, 960–971.
- 789 Francese, R., Mazzarini, F., Bistacchi, A.L.P., Morelli, G., Pasquare, G., Praticelli, N.,
790 Robain, H., Wardell, N., Zaja, A., 2009. A structural and geophysical approach to the study
791 of fractured aquifers in the Scansano-Magliano in Toscanaridge, southern Tuscany, Italy.
792 *Hydrogeology Journal*, 17,1233–1246
- 793 Fuh, S.C., Liu, H.C., Ku, C.Y., Chang, T.Y., 2019. 1D Vertical electrical sounding method
794 applied to evaluate shallow gas potential associated with the Hsinying and the Niushan
795 fields in SW Taiwan. *SEG International Exposition and 89th Annual Meeting*, 1179-1183.
796 10.1190/segam2019-3200645.1
- 797 Geoscan-M Ltd., 2001. IPI2Win v.2.1, IPI_Res2, IPI_Res3 User's Guide. Moscow State
798 University, 25p.
- 799 Ghosh, D.P., 1971. The application of linear filter theory on the direct interpretation of
800 geoelectrical resistivity sounding measurements. *Geophysical Prospecting*, 19, 192–217.
- 801 Gupta, P.K., Nirwas, S., Gaur, V.K., 1997. Straightforward inversion of vertical electrical
802 sounding data. *Geophysics*, 62(3), 775–785. <https://doi.org/10.1190/1.1444187>
- 803 Hafid, M., 2000. Triassic-early Liassic extensional systems and Tertiary inversion, Essaouira
804 Basin (Morocco). *Marine and Petroleum Geology*, 17, 409-429.
- 805 Himi, M., Tapias, J., Benabdelouahab, S., Salhi, A., Rivero, L., Elgettafi, M., El Mandour, A.,
806 Stitou, J., Casas, A., 2017. Geophysical characterization of saltwater intrusion in a coastal
807 aquifer: The case of Martil-Alila plain (North Morocco). *Journal of African Earth*
808 *Sciences*, 126, 136-147. <https://doi.org/10.1016/j.jafrearsci.2016.11.011>
- 809 Hodlur, G.K, Dhakate, R., Andrade, R., 2006. Correlation of vertical electrical sounding and
810 borehole-log data for delineation of saltwater and freshwater aquifers. *Geophysics*, 71(1),
811 G11–G20. <https://doi.org/10.1190/1.2169847>
- 812 Karroum, M., El Guettafi, M., El Mandour, A., Wilske, C., Himi, M., Casas, A., 2017.
813 Geochemical processes controlling groundwater quality under semi-arid environment: A

- 814 case study in central Morocco. *Science of the Total Environment*, 609, 1140-1151.
815 <https://dx.doi.org/10.1016/j.scitotenv.2017.07.199>
- 816 Kosinky, W.K., Kelly, W.E., 1981. Geoelectrical sounding for predicting aquifer properties.
817 *Groundwater*, 19, 163-171.
- 818 Kumar, D., Rao, V.A., Nagaiah, E., Raju, P.K., Mallesh, D., Ahmeduddin, M., Ahmed,
819 S.,2010. Integrated geophysical study to decipher potential groundwater and zeolite-
820 bearing zones in Deccan Traps. *Current Science*, 98(6),803–814.
- 821 Kumar, D., Rao, V.A., Sarma, V.S., 2014. Hydrogeological and geophysical study for deeper
822 groundwater resource in quartzitic hard rock ridge region from 2D resistivity data. *Journal*
823 *of Earth System Science*, 123(3), 531–543.
- 824 Mashhad, S.R., Ramazi, H., Asgarpour Shahreza, M., 2020. Assessing the effects of 1D
825 assumption violation in vertical electrical sounding (VES) data processing and
826 interpretation. *Acta Geophysica*. <https://doi.org/10.1007/s11600-019-00384-1>
- 827 Mader, N.K., Redfern, J., El Ouataoui, M., 2017. Sedimentology of the Essaouira Basin
828 (Meskala Field) in context of regional sediment distribution patterns during upper Triassic
829 pluvial events. *Journal of African Earth Sciences*, 130, 293-318.
- 830 Manu, E., Agyekum, W.A., Duah, A.A., Mainoo, P.A., Okrah, C., Asare, V.S., 2016.
831 Improving Access to Potable Water Supply using Integrated Geophysical Approach in a
832 Rural Setting of Eastern Ghana. *Elixir Environ. & Forestry*, 95, 40714-40719.
- 833 Mazac, O., Kelly, W.E., Landa, I., 1985. A hydrophysical model for relation between
834 electrical and hydraulic properties of aquifers. *Journal of Hydrology*, 79, 1-19.
- 835 Medina, F., 1994. Evolution structurale de Haut Atlas Occidental et des régions voisines du
836 Trias à l'actuel, dans le cadre de l'ouverture de l'Atlas Atlantique Centrale et de la
837 collision Afrique-Europe. *Thèse de Doctorat ès-Sciences*, Université Mohammed V, Rabat,
838 Morocco, 272p.
- 839 Mennani, A., 2001. Apport de l'Hydrochimie et de l'Isotopie à la connaissance du
840 fonctionnement des aquifères de la zone côtière d'Essaouira (Maroc occidental). *Thèse de*
841 *Doctorat ès-Sciences*, Université Cadi Ayyad, Marrakech, Morocco, 172p.
- 842 Ogungbe, A.S., Onori, E.O., Olaoye, M.A., 2012. Application of electrical resistivity
843 techniques in the investigation of groundwater contamination. A case study of ille-Epo
844 Dumpsite, Lagos, Nigeria. *International Journal of Geomatics and Geosciences*, 3(1), 30-
845 41.

- 846 Okrah, C., Danuor, S.K., Dapaah-Siakwan, S., 2012. Groundwater exploration in granitic rock
 847 formation of Komenda/Edina/Eguafo/Abirem district using integrated geophysical
 848 techniques. *Journal of the Ghana Science Association*, 14(2), 56–72.
- 849 Ouhamdouch, S., Bahir, M., Ouazar, D., 2021. Seawater intrusion into coastal aquifers from
 850 semi- arid environments, Case of the alluvial aquifer of Essaouira basin (Morocco).
 851 *Carbonates and Evaporites*, 36, 5. <https://doi.org/10.1007/s13146-020-00663-9>
- 852 Ouhamdouch, S., Bahir, M., Carreira, P.M., 2018. Impact du changement climatique sur la
 853 ressource en eau en milieu semi-aride : exemple du bassin d'Essaouira (Maroc). *Revue des*
 854 *Sciences de l'eau*, 31(1), 13-27. <https://doi.org/10.7202/1047050ar>
- 855 Ouzerbane, Z., Najine, A., Aïfa, T., El Hmaid, A., Essahlaoui, A., Redouani, F., 2013. Etude
 856 géophysique par imagerie électrique du système aquifère au Nord-Est du bassin
 857 d'Essaouira, Maroc. *Journal of Hydrocarbons, Mines and Environmental Research*, 4(1),
 858 57-70.
- 859 Ouzerbane, Z., Najine, A., Aïfa, T., El Hmaid, A., Essahlaoui, A., 2014. Apport de
 860 l'hydrogéophysique et le SIG à l'étude des ressources en eaux dans la partie nord côtière
 861 du bassin d'Essaouira-Maroc. *Colloque international des Utilisateurs de SIG, TAZA GIS-*
 862 *Days, Morocco. Infrastructure des données spatiales et Application des SIG*, 300-306.
 863 ISBN : 978-3-8381-4837-3.
- 864 Ouzerbane, Z., 2015. Contribution de la géophysique, des SIG et de l'analyse multicritère à la
 865 reconnaissance des ressources en eau et leur vulnérabilité à la pollution. Cas du sous-bassin
 866 côtier d'Essaouira (Maroc). *Thèse de Doctorat*, Université Moulay Ismail, Meknès,
 867 Morocco, 304p.
- 868 Ouzerbane, Z., Boughalem, M., El Hmaid, A., Essahlaoui, A., Najine, A., Aïfa, T., Redouani,
 869 F., El Ouali, A. 2018. Evaluation des facteurs physiographiques et leurs impacts sur les
 870 ressources en eau dans les bassins versants d'Essaouira (Essaouira, Maroc). *Journal*
 871 *International Sciences et Technique de l'Eau et de l'Environnement*, 3(1), 29-37. ISSN
 872 (electronic): 1737-9350; ISSN (printed): 1737-6688.
- 873 Ouzerbane, Z., El Hmaid, A., Essahlaoui, A., Najine, A., Aïfa, T., Abbassi, M., El Ouali, A.,
 874 2018. Application de la méthode DRASTIC à l'étude de la vulnérabilité à la pollution des
 875 aquifères dans la zone côtière d'Essaouira (Essaouira, Morocco). *4^{ème} édition du Colloque*
 876 *international des Utilisateurs des SIG (Meknès GISDAYS2018)*. Université Moulay Ismail,
 877 Faculté des Sciences, p. 141, Meknès, 20 – 21 décembre 2018.
- 878 Ouzerbane, Z., Boughalem, M., El Hmaid, A., Aïfa, T., Essahlaoui, A., El Ouali, A., Najine
 879 A., Redouani, F., Wafik, A., 2019. Application of GIS to study the physiographic factors

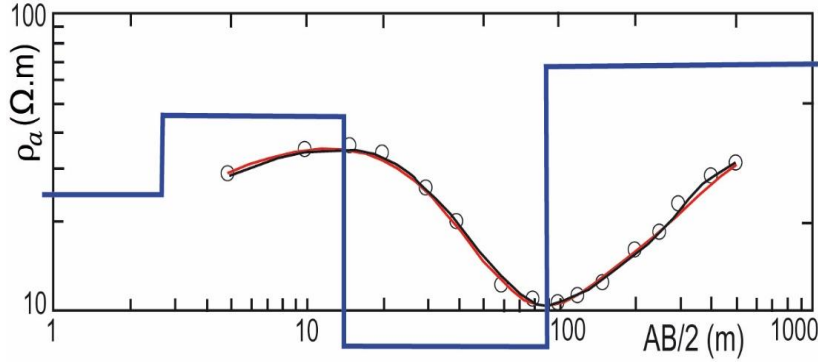
- 880 and the water resources in the watersheds of Essaouira, Morocco. *Journal of Water*
 881 *Sciences & Environment Technologies*, 4(1), 480-490, ISSN: 2508-9250,
- 882 Owen, R.J., Gwavava, O., Gwaze, P., 2005. Multi-electrode resistivity survey for
 883 groundwater exploration in the Harare greenstone belt, Zimbabwe. *Hydrogeology Journal*,
 884 14, 244-252. <https://doi.org/10.1007/s10040-004-0420-7>
- 885 Perrone, A., Iannuzzi, A., Lapenna, V., Lorenzo, P., Piscitelli, S., Rizzo, E., Sdao, F., 2004.
 886 High resolution electrical imaging of the Varco d'Izzo earthflow (Southern Italy). *Journal*
 887 *of Applied Geophysics*, 56, 17–29.
- 888 Piatti, C., Boiero, D., Godio, A., Socco, L.V., 2010. Improved Monte Carlo 1D inversion of
 889 vertical electrical sounding and time-domain electromagnetic data. *Near Surface*
 890 *Geophysics*, 8, 117-133.
- 891 Piqué, A., 1994. Géologie du Maroc. Les domaines régionaux et leur évolution structurale.
 892 *Presses Universitaires Maghrébines Edition*, Marrakech, Morocco, 284p.
- 893 Piqué, A., Laville, E., 1996. The central Atlantic rifting: reactivation of Palaeozoic structures?
 894 *Journal of Geodynamics*, 21, 235-255. Piqué, A., Le Roy, P., Amrhar, M., 1998.
 895 Transpressive synsedimentary tectonics associated with ocean opening: the Essaouira-
 896 Agadir segment of the Moroccan Atlantic margin. *Journal of the Geological Society*,
 897 *London*, 155, 913-928.
- 898 Redouani, F., Najine, A., Aïfa, T., Ouzerbane, Z., 2013. Reconnaissance du système aquifère
 899 du nord-ouest de la plaine du Tadla (Maroc central) par imagerie électrique. *Journal of*
 900 *Hydrocarbons, Mines and Environmental Research*, 4(1), 33-41.
- 901 Sainato, C., Galindo, G., Pomposiello, C., Malleville, H., de Abelleira, D., Lossino, B., 2003.
 902 Electrical conductivity and depth of groundwater at the Pergamino zone (Buenos Aires
 903 Province, Argentina) through vertical electrical sounding and geostatistical analysis.
 904 *Journal of South American Earth Sciences*, 161, 177–186.
 905 [https://dx.doi.org/10.1016/S0895-9811\(03\)00027-0](https://dx.doi.org/10.1016/S0895-9811(03)00027-0)
- 906 Sajinkumar, K.S., Castedo, R., Sundarajan, P., Rani, V.R., 2015. Study of a partially failed
 907 landslide and delineation of piping phenomena by vertical electrical sounding (VES) in the
 908 Wayanad Plateau, Kerala, India. *Natural Hazards*, 75, 755–778.
 909 <https://doi.org/10.1007/s11069-014-1342-x>
- 910 Sharma, P.V., 1997. Environmental and engineering geophysics. *Cambridge University Press*,
 911 475p.

- 912 Sharma, S.P., Baranwal, V.C., 2005. Delineation of groundwater-bearing fracture zones in a
913 hard rock area integrating very low frequency electromagnetic and resistivity data. *Journal*
914 *of Applied Geophysics*, 57, 155-166. <https://doi.org/10.1016/j.jappgeo.2004.10.003>
- 915 Sherif, M., El Mahmoudi, A., Garamoon, H., Shetty, A., 2006. Geoelectrical and
916 hydrogeochemical studies for delineating seawater intrusion in the outlet of Wad, Ham,
917 UAE. *Environmental Geology*, 49, 536–551
- 918 Sikah, J.N., Aning, A.A., Danuor, S.K., Manu, E., Okrah, C., 2016. Groundwater Exploration
919 using 1D and 2D Electrical Resistivity Methods. *Journal of Environmental Earth Science*,
920 6(7), 55-63.
- 921 Sinan, M., Boussetta, M., El Rherari, A., 2009. Changements climatiques : Causes et
922 conséquences sur le climat et les ressources en eau. Séminaire international sur : Le
923 dessalement des eaux. *Recueil des communications, Amicale des Ingénieurs du Génie*
924 *Rural du Maroc*, Tanger, Morocco, 12-22.
- 925 Singh, U.K., Tiwari, R.K., Singh, S.B., 2005. One-dimensional inversion of geo-electrical
926 resistivity sounding data using artificial neural networks—a case study. *Computers and*
927 *Geosciences*, 31, 99-108. <https://doi.org/10.1016/j.cageo.2004.09.014>
- 928 Singh, U.K., Tiwari, R.K., Singh, S.B., 2013. Neural network modeling and prediction of
929 resistivity structures using VES Schlumberger data over a geothermal area. *Computers and*
930 *Geosciences*, 52, 246-257. <https://dx.doi.org/10.1016/j.cageo.2012.09.018>
- 931 Souid, A., 1983. Etude tectonique et microtectonique des injections du Trias dans le bassin
932 d'Essaouira pendant les compressions alpines dans l'avant-pays atlasique (Maroc). *Thèse*
933 *de Doctorat 3^{ème} cycle*, Université de Montpellier, France, 101p.
- 934 Srinivas, Y., Raj, A.S., Oliver, H.D., Muthuraj, D., Chandrasekar, N., 2012. A robust
935 behavior of Feed Forward Back propagation algorithm of Artificial Neural Networks in the
936 application of vertical electrical sounding data inversion. *Geoscience Frontiers*, 3(5), 729-
937 736. <https://dx.doi.org/10.1016/j.gsf.2012.02.003>
- 938 Store, H., Storz, W., Jacobs, F., 2000. Electrical resistivity tomography to investigate
939 geological structures of Earth's upper crust. *Geophysical Prospecting*, 48,455–471.
- 940 Taj-Eddine, K., 1991. Le Jurassique terminal et le Crétacé basal dans l'Atlas Atlantique
941 (Maroc), Biostratigraphie, Sédimentologie, Stratigraphie séquentielle et Géodynamique.
942 *Thèse de Doctorat ès-Sciences*, Université Cady Ayyad, Marrakech, Morocco, 285p.
- 943 Urish, D.W., Frohlich, R.K., 1990. Surface electrical resistivity in coastal groundwater
944 exploration. *Geoexploration*, 26, 267–289.

- 945 Wafiq, A., Ec-Chouafi, E., Didi, S., Ouzerbane, Z., Abbari, M., 2019. Hydro-electric study of
946 Bajocian aquifer of Mellaha village, Oued Guir, Errachidia, Morocco. *Journal of Water*
947 *Sciences & Environment Technologies*, 4(1), 428-442. ISSN: 2508-9250.
- 948 Yadav, G.S., Singh, S.K., Srivastava, K.M., 1997. Fast method of resistivity sounding for
949 shallow groundwater Investigations. *Journal of Applied Geophysics*, 36, 45-52.
- 950 Yadav, G.S., Abolfazli, H., 1998. Geoelectrical soundings and their relationships to Hydraulic
951 parameters in semiarid regions of Jalore, North West India. *Journal of Applied Geophysics*,
952 39, 35-51.
- 953 Yadav, G.S., Singh, S.K., 2007. Integrated resistivity surveys for delineation of fractures for
954 ground water exploration in hard rock area. *Journal of Applied Geophysics*, 62(3), 301–
955 312.
- 956 Zaidi, F.K., Kassem, O.M.K., 2012. Use of electrical resistivity tomography in delineating
957 zones of groundwater potential in arid regions; a case study from Diriyah region of Saudi
958 Arabia. *Arabian Journal of Geosciences*, 5, 327–333.
- 959 Zhody, A., 1989. A new method for the interpretation of Schlumberger and Wenner sounding
960 curves. *Geophysics*, 54(2), 245–253.

Table 1

VES site	X	Y	Z	Type	ρ (Ω .m)	H (m)	D (m)	Error (%)
28	109247	121120	204	A	25 45 8 68	3 11 75	3 14 89	3.25

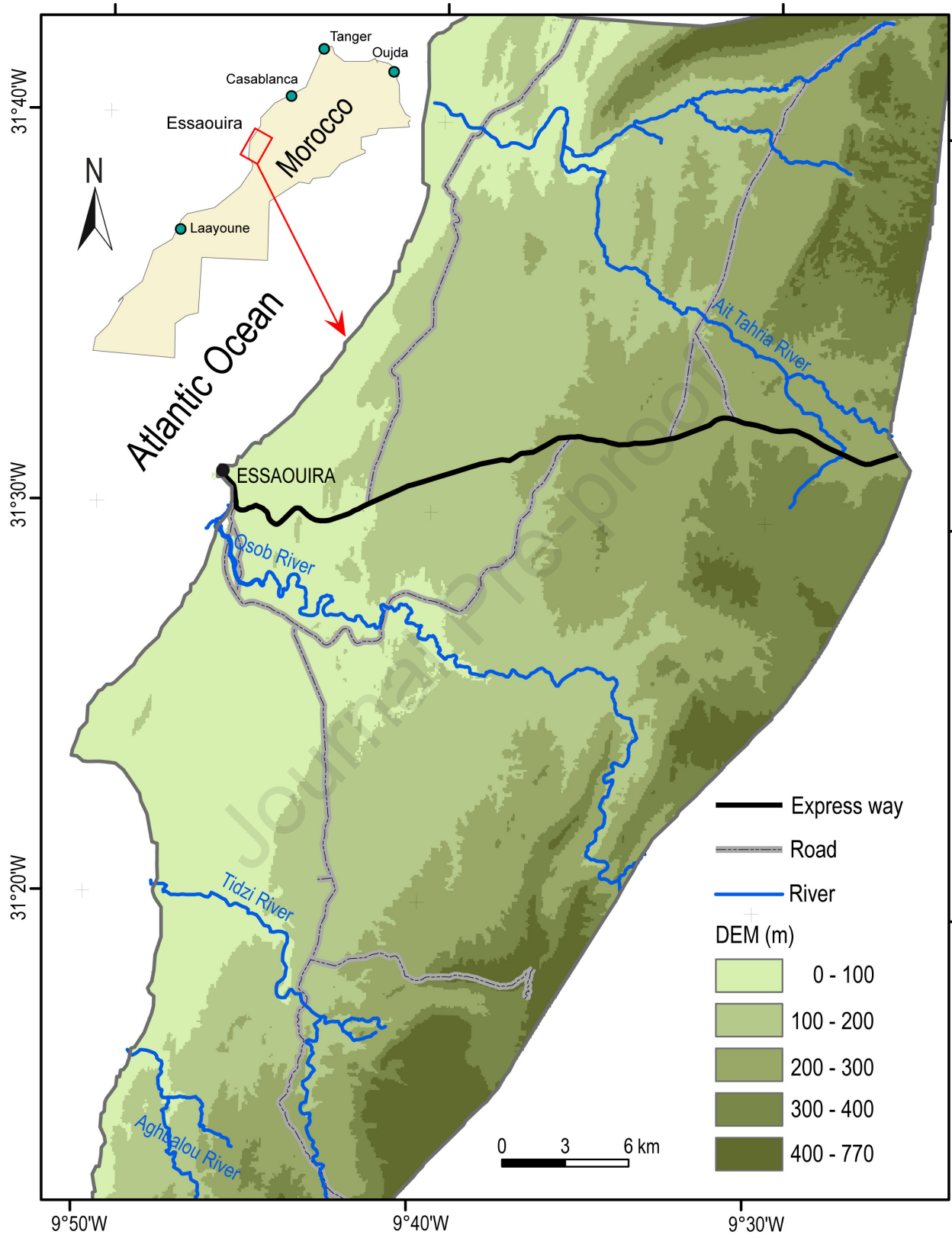


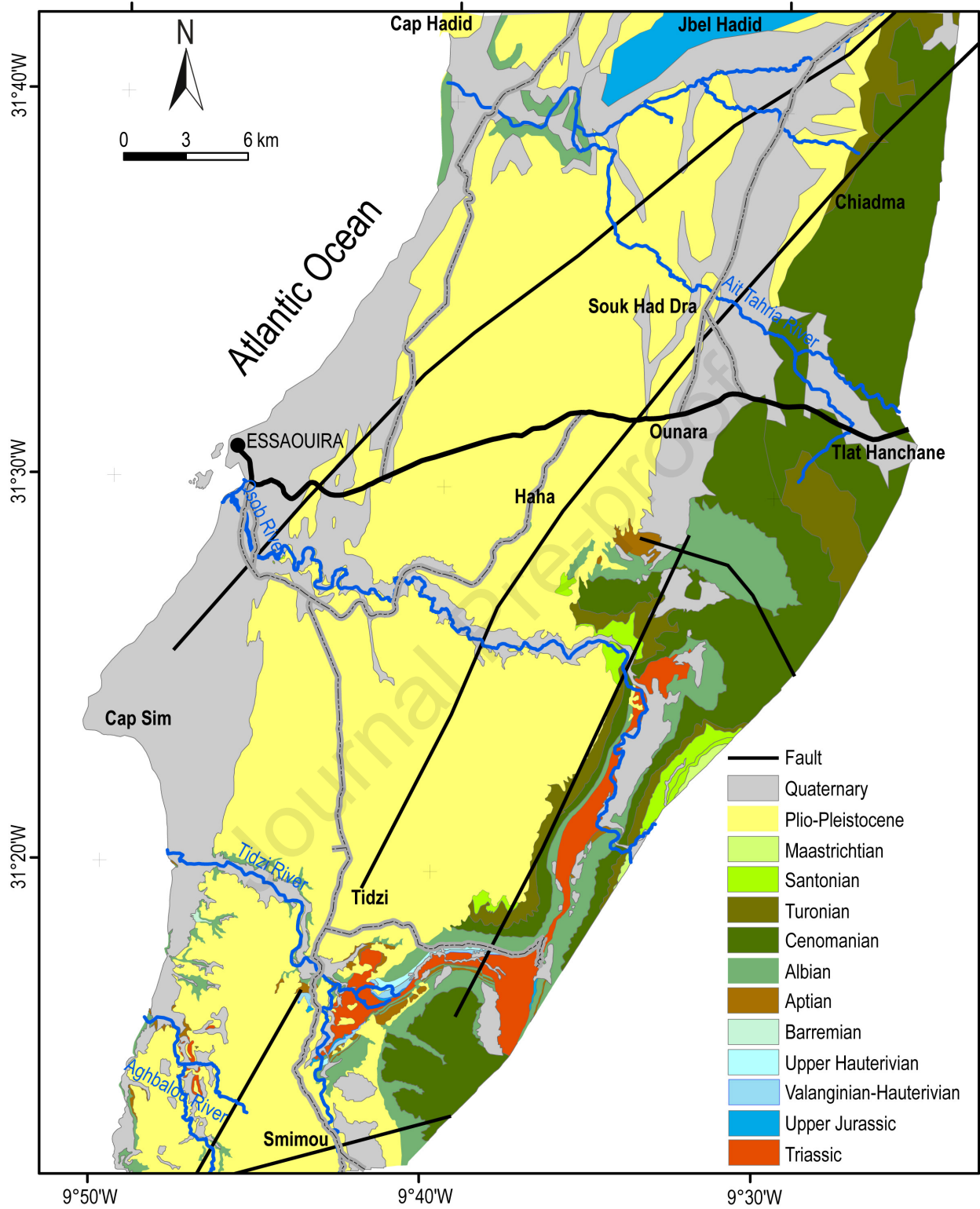
VES	Family type	Roof depth (m)	Wall depth (m)	Lithology	Age	Thickness (m)	ρ (Ω .m)
VES2	A	0.	1.7	Sand	Plio-Pleistocene	1.7	257
		1.7	4.7	Sandy marl	Plio-Pleistocene	3	57
		4.7	45.7	Marl	Cenomanian	41	19
		45.7	147.2	Marly limestone	Cenomanian	101.5	50
VES4	A	0	8	Sandy marl	Plio-Pleistocene	8	69
		8	46	Marl	Cenomanian	38	15
		46	134	Marly limestone	Cenomanian	88	60
VES17	B	0	2	Sand	Plio-Pleistocene	2	206
		2	29	Wet sand	Plio-Pleistocene	27	68
		29	88	Wet sandstone	Plio-Pleistocene	59	182
VES21	B	0	6	Marl	Cenomanian	6	32
		6	63	Marl	Cenomanian	57	47
		63	143	Marly limestone	Cenomanian	80	88
VES40	C	0	4	Sand	Plio-Pleistocene	4	224
		4	52	Wet sand	Plio-Pleistocene	48	89
		52	158	Marl and marly limestone	Santonian	106	57
SE57	C	0	8	Silt	Plio-Pleistocene	8	24
		8	52	Flint limestone	Barremian-Albian	44	98
		52	115	Marl	Barremian-Albian	63	15

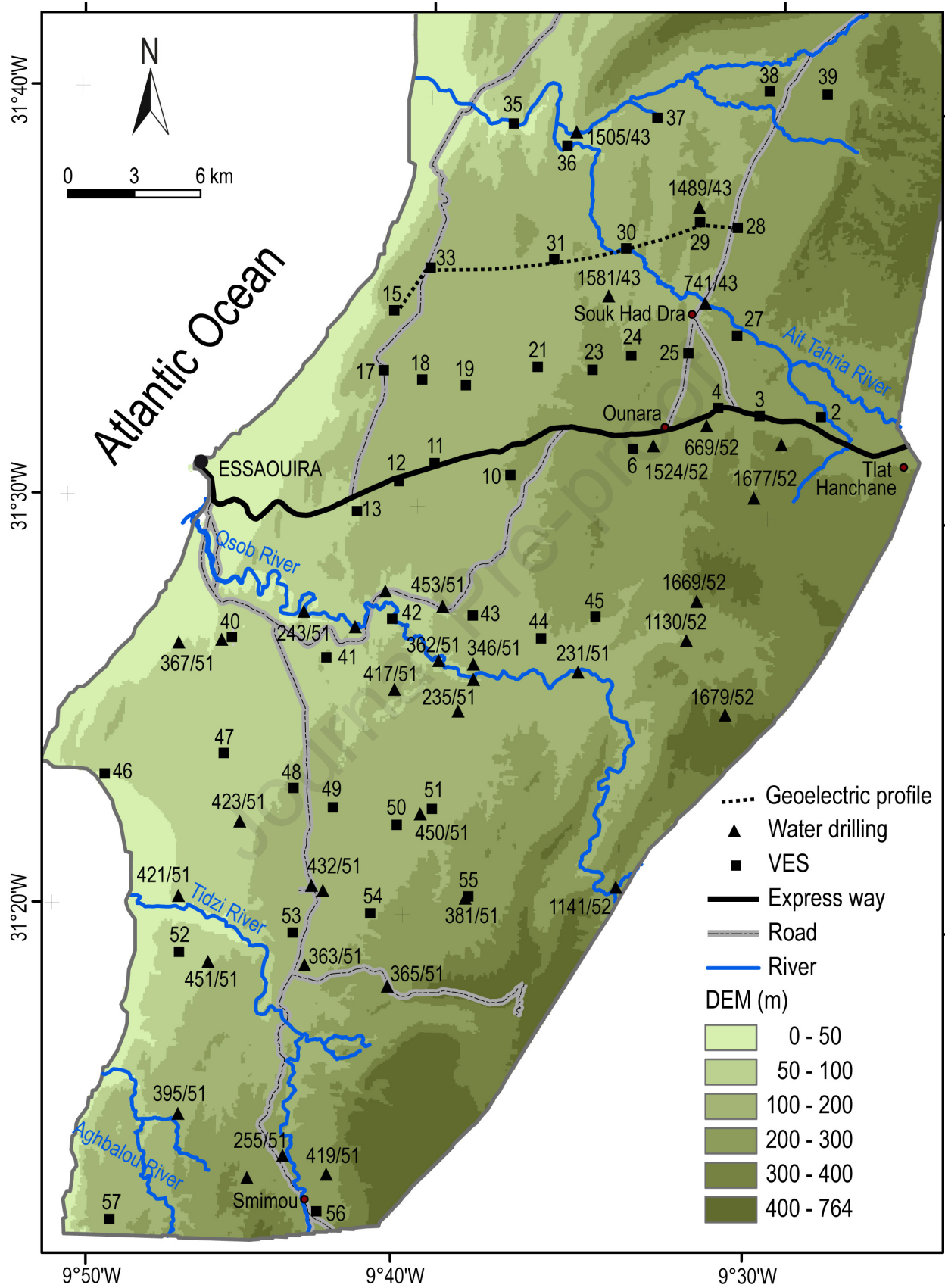
Well (W)/Source (S)	Site location	X	Y	Z	WH (m)	PL (m)	T (°C)	pH	EC ($\mu\text{S/cm}$)
W1	Lgoutra	113301	111587	273	17.5	255.5	22.6	4.18	3982
W2	Ait Abdessalam	114002	111622	269	12.0	257.0	22.2	8.60	3604
W3	Ait Louafi	114256	111258	273	33.4	239.6	23.2	6.43	3772
W4	Ait Hida	113358	112545	265	36.0	229.0	22.5	6.61	4000
W5	Boujlakh	108482	113349	242	37.5	204.5	22.5	7.23	3333
W6	Boujlakh	108291	113042	244	37.0	207.0	23.8	6.37	3361
W7	Ait Hmad	106416	112420	223	30.6	192.4	23.5	7.00	3298
W8	Ait Hmad	106785	112222	225	28.0	197.0	22.9	8.23	2838
W9	Lahrarta	99631	110099	210	53.3	156.7	23.7	6.45	3376
W10	Lahrarta	99488	110225	217	65.5	151.5	25.9	7.80	2703
W11	Lahrarta	98840	110264	213	80.0	133.0	25.4	7.60	1969
W12	Lahrarta	98474	110964	203	63.5	139.5	26.1	8.72	2586
W13	Laarab	91904	108273	109	57.4	51.6	23.0	8.13	1522
W14	Laarab	91464	108577	108	51.0	57.0	22.3	7.08	3027
W15	Loubane	91720	111175	121	74.3	46.7	23.9	6.40	2510
W16	Laarab	91559	109501	108	87.0	21.0	22.8	6.70	2083
W17	Laaraych	92800	114626	129	87.0	42.0	27.2	7.90	4320
W18	Laaraych	93035	114559	123	61.0	62.0	23.0	7.93	2391
W19	Laaraych	92724	112184	125	72.0	53.0	24.3	8.50	1955
W20	Laaraych	92024	112283	106	60.0	46.0	23.4	8.39	2885
W21	El Kouach	98761	114362	156	39.3	116.7	26.0	8.20	1346
W22	El Kouach	98856	114421	152	33.0	119.0	23.9	7.23	2510
W23	Ougdila	100092	114900	168	47.0	121.0	23.8	7.90	1261
W24	Tiglat	100292	114523	183	53.2	129.8	24.0	7.80	1875
W25	Tiglat	100598	113599	197	49.0	148.0	23.6	7.08	1483
W26	Tabya	108415	116287	216	15.3	200.7	22.8	7.56	2961
W27	Tabya	108463	116160	221	17.4	203.6	22.7	7.02	2974

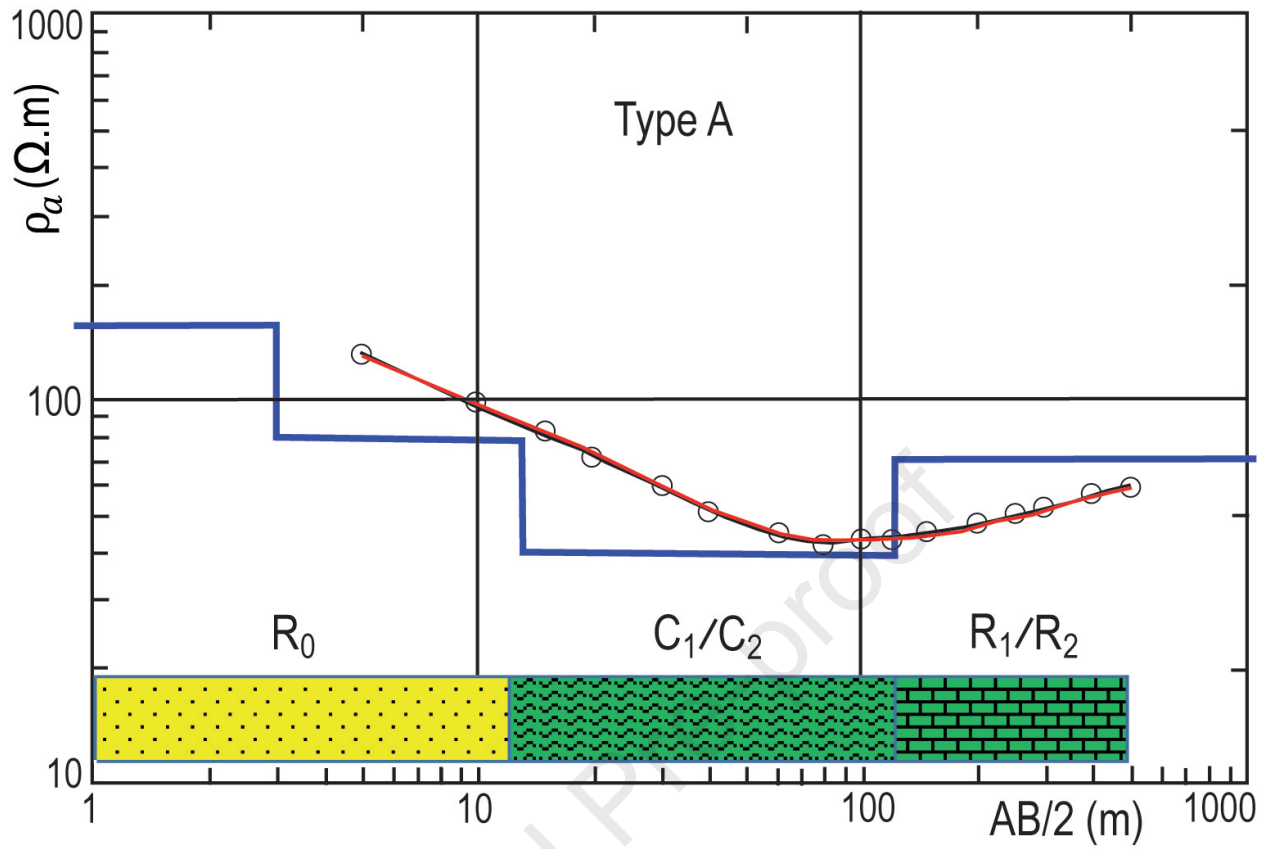
W28	Tabya	108602	115959	218	18.5	199.5	22.8	6.74	2632
W29	Chebabta	109245	115676	219	20.0	199.0	22.7	8.80	3304
W30	Matrazza	109254	121141	216	15.5	200.5	22.7	8.30	6278
W31	Matrazza	110259	120150	214	20.5	193.5	22.6	7.70	5310
W32	Nguiaa	107559	121921	211	27.0	184.0	21.8	8.40	3555
W33	Nguiaa	107548	122023	217	31.0	186.0	22.1	7.80	5656
W34	Nguiaa	107636	121905	203	25.0	178.0	22.0	6.90	6818
W35	Amarat	106947	119576	203	16.0	187.0	22.5	8.30	7111
W36	Imzoughar	101538	119052	187	68.0	119.0	24.2	7.60	3202
W37	Imzoughar	101139	118552	178	54.8	123.2	23.5	6.80	3830
W38	Imzoughar	100975	118189	176	52.5	123.5	23.6	8.60	1695
W39	Bouchaaib	99897	116598	163	49.0	114.0	23.4	6.40	2030
W40	Wlage Sidi Bouzakri	94546	124969	19	10.0	9.0	21.5	8.07	4395
W41	Ait Tahriya	98704	125749	43	11.5	31.5	21.8	8.18	3589
W42	Ait Tahriya	99113	125844	48	14.0	34.0	23.9	8.13	4916
W43	Agadir	102135	125566	115	100.0	15.0	25.0	8.30	2220
S1	Ain Lahjar	103132	124571	100	0.0	100.0	22.3	8.40	4641
W44	Sidi Yahia	105544	126217	145	4.3	140.7	23.3	8.30	3938
S2	Ain Lkhatarat	105167	126407	127	0.0	127.0	24.4	8.30	4232
W45	Ait Himouch	113980	126990	284	120.0	164.0	26.2	8.34	3015
W46	Ait Laarbi	114081	126486	279	70.0	209.0	26.2	8.31	4103
W47	Takkat	114415	124547	282	5.6	276.4	21.5	8.22	3186
W48	Imi Ntagant	86914	101829	80	20.0	60.0	22.2	8.30	3536
W49	Imi Ntagant	86911	101696	72	20.0	52.0	22.5	8.30	3478
W50	Ait Achouayakh	90738	101920	107	36.0	71.0	22.3	8.30	2859
W51	Ait Achouayakh	90440	101980	107	46.0	61.0	22.8	8.30	2950
W52	Zaouit Sidi Brahim	93633	103430	90	18.0	72.0	21.6	8.40	2326
W53	Tazitounte	86047	97636	66	7.0	59.0	21.0	8.40	6536
W54	Id Zaouit	95472	88396	263	46.0	217.0	23.0	8.40	1924

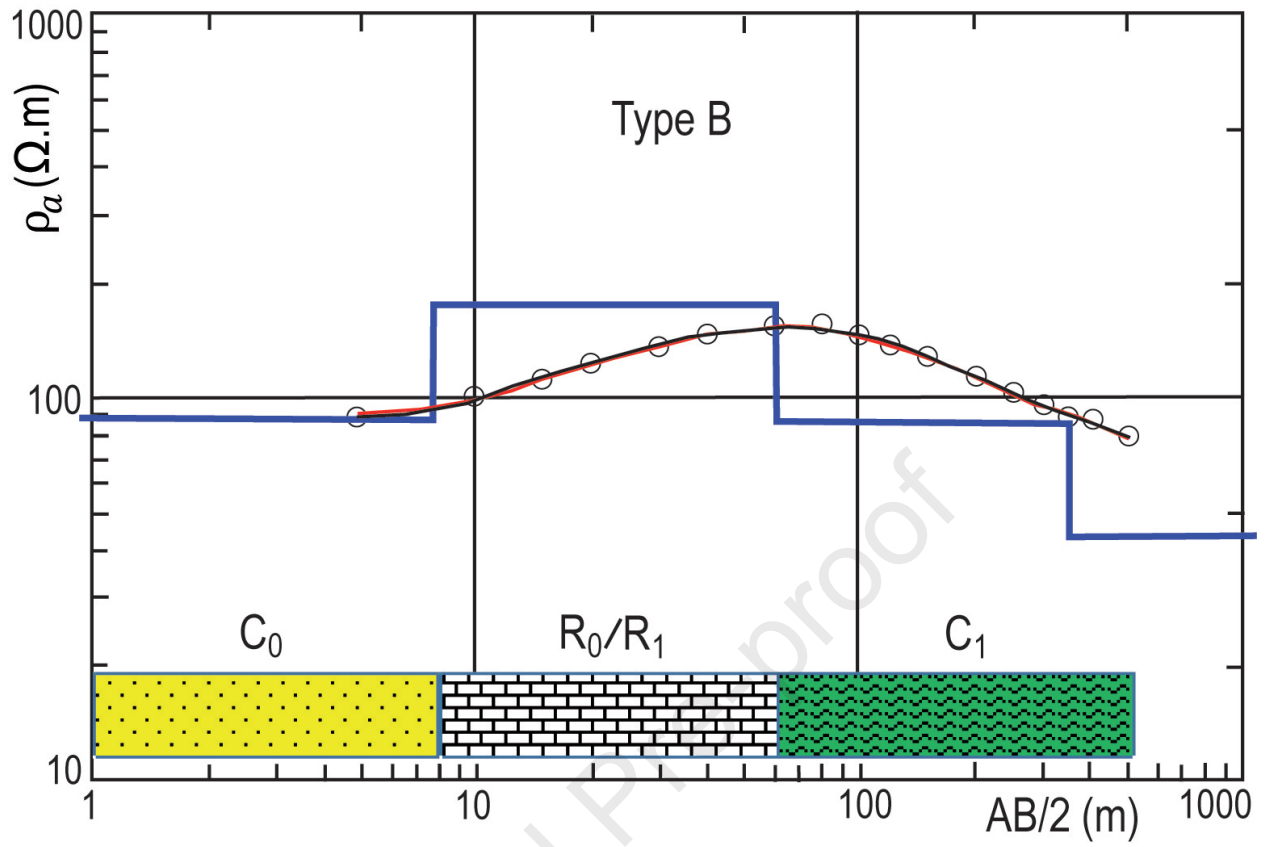
W55	Ikaabar	95527	90821	200	29.0	171.0	22.3	8.08	1009
S3	Ain Tassakra	83872	80561	175	0.0	175.0	23.1	8.12	2413
S4	Ain Aghbalou	83380	80749	89	0.0	89.0	23.4	8.35	3376
W56	Id Amar	99626	109044	188	17.3	170.7	23.4	8.21	611
W57	Hrarta	99027	107695	162	8.0	154.0	23.7	8.07	1973
W58	Ichbak 1	98547	106176	144	5.5	138.5	21.1	8.34	3957
W59	Ichbak 2	97048	104906	135	34.3	100.7	22.7	8.62	2985
W60	Sahli	95736	104124	113	30.5	82.5	23.0	8.04	6293
W61	-	90185	100586	104	40.0	64.0	22.5	8.30	1883
W62	Tidzi	89380	88397	132	24.0	108.0	23.1	8.47	3333
W63	Smimou	89655	77479	259	5.0	254.0	22.2	8.63	1417
W64	Diabat	85109	105776	43	37.2	5.8	23.4	6.36	3160
W65	Ait Moumen	89298	98612	94	38.0	56.0	22.7	6.51	2510
W66	Zaouit Sidi Brahim	93416	102734	103	47.0	56.0	20.8	6.60	1680
W67	Sidi Ali Bazour	93656	100268	100	34.0	66.0	23.6	6.58	1680
W68	Zaouit Sidi Brahim	94534	102323	98	22.5	75.5	21.4	6.56	1610
W69	Sidi Kawki	82006	93200	14	4.0	10.0	23.3	6.52	2120
W70	Echaabat	90156	95296	119	61.0	58.0	21.3	6.60	1920
W71	Sidi Hmad Ou Hmad	89402	91160	130	28.0	102.0	23.4	6.27	5780
W72	Id Kaddour	87980	79808	240	39.0	201.0	22.7	6.33	3350
W73	Smimou	89678	76643	257	6.0	251.0	22.4	6.30	1610
W74	Bou Tazert	87745	95875	90	5.0	85.0	23.2	6.50	3530

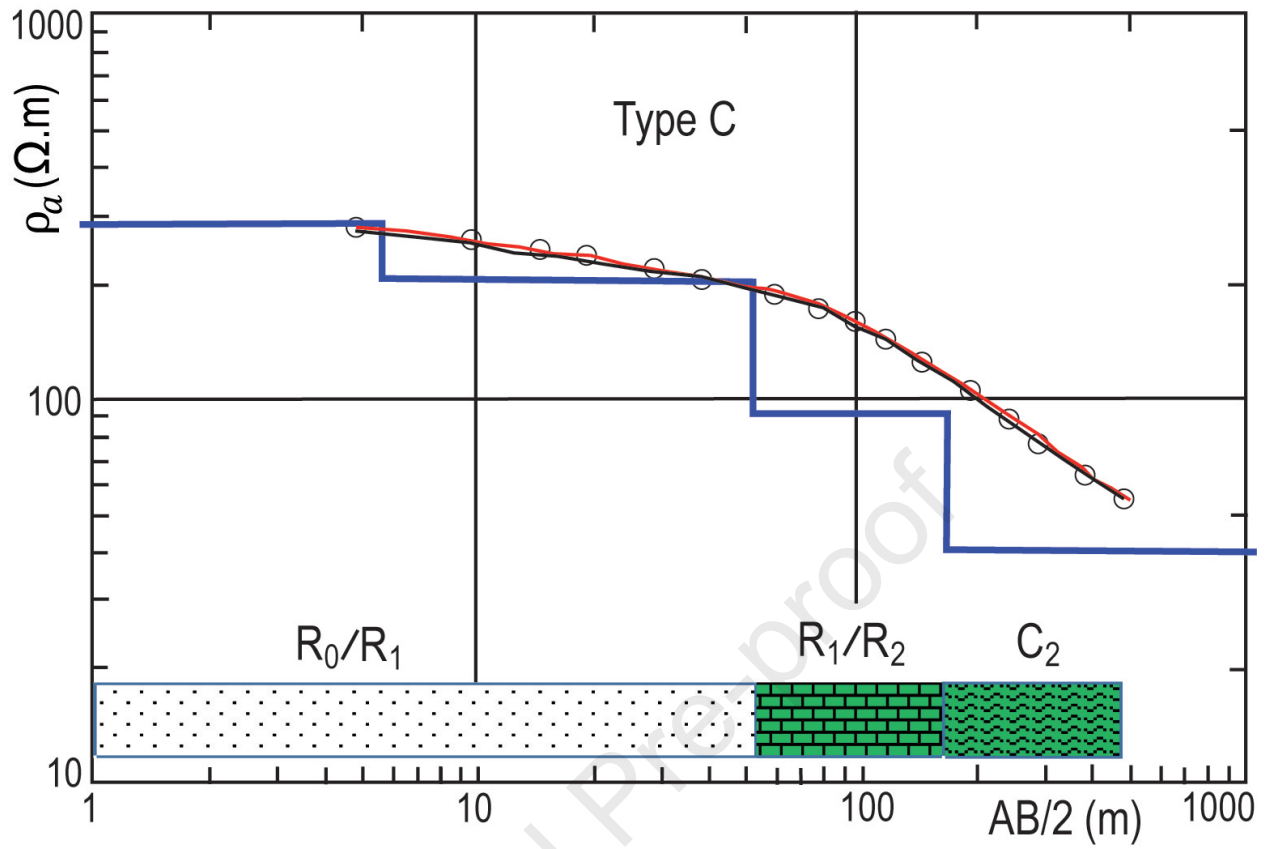


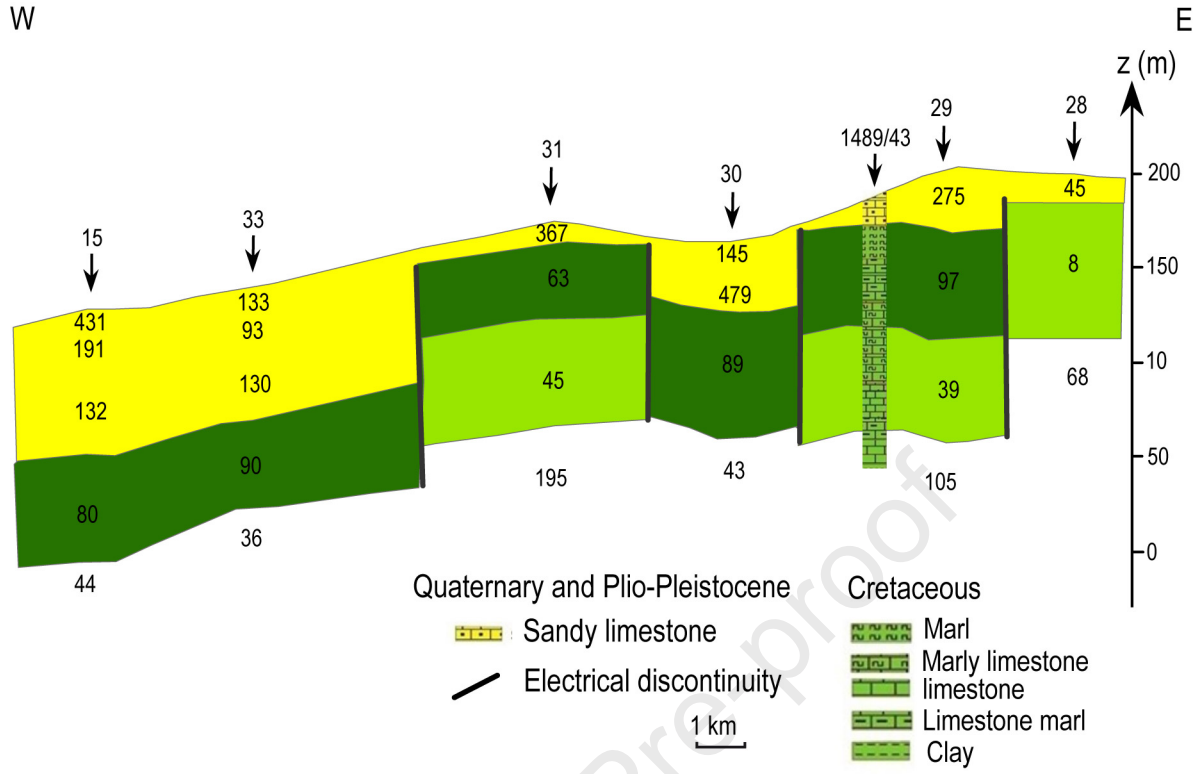


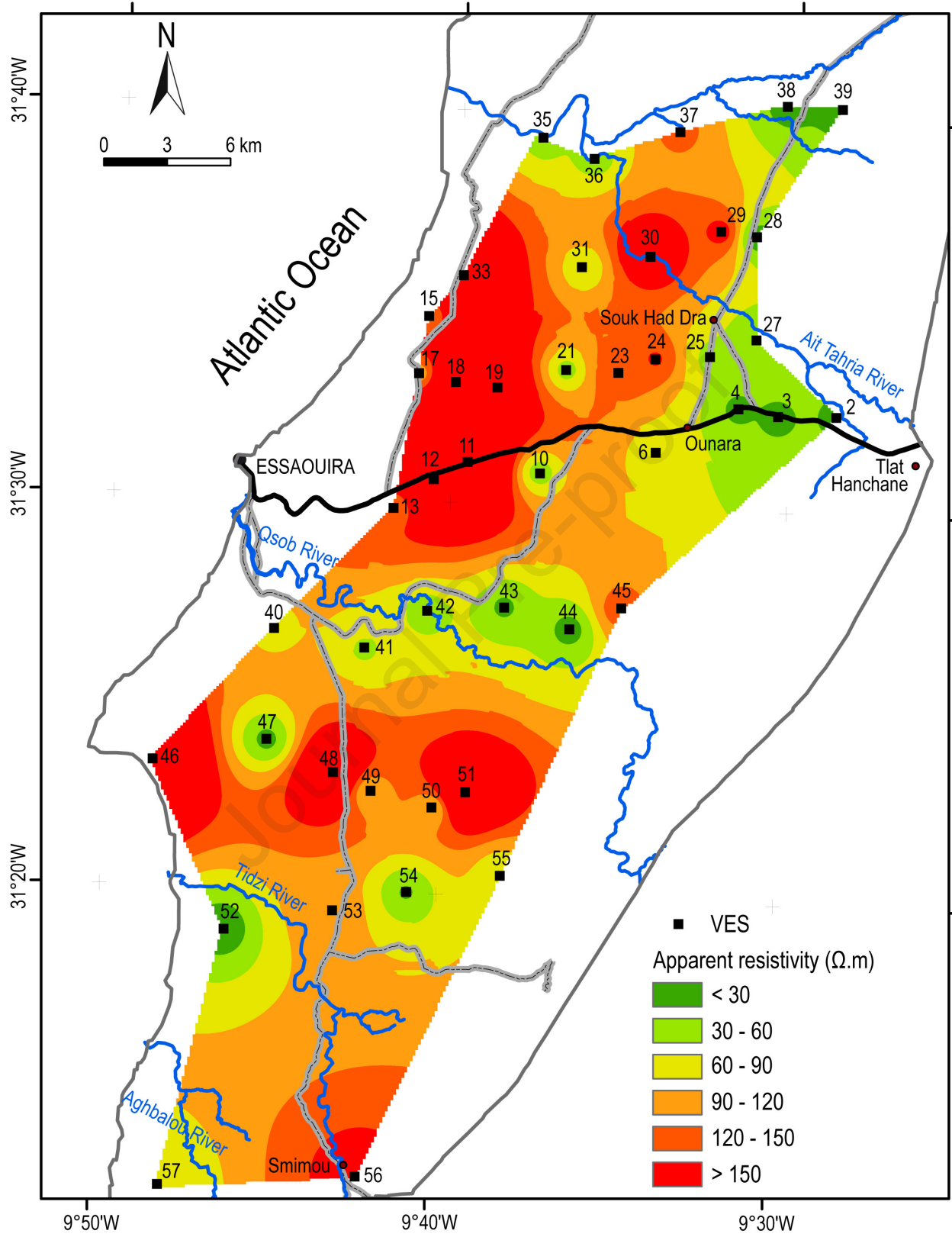


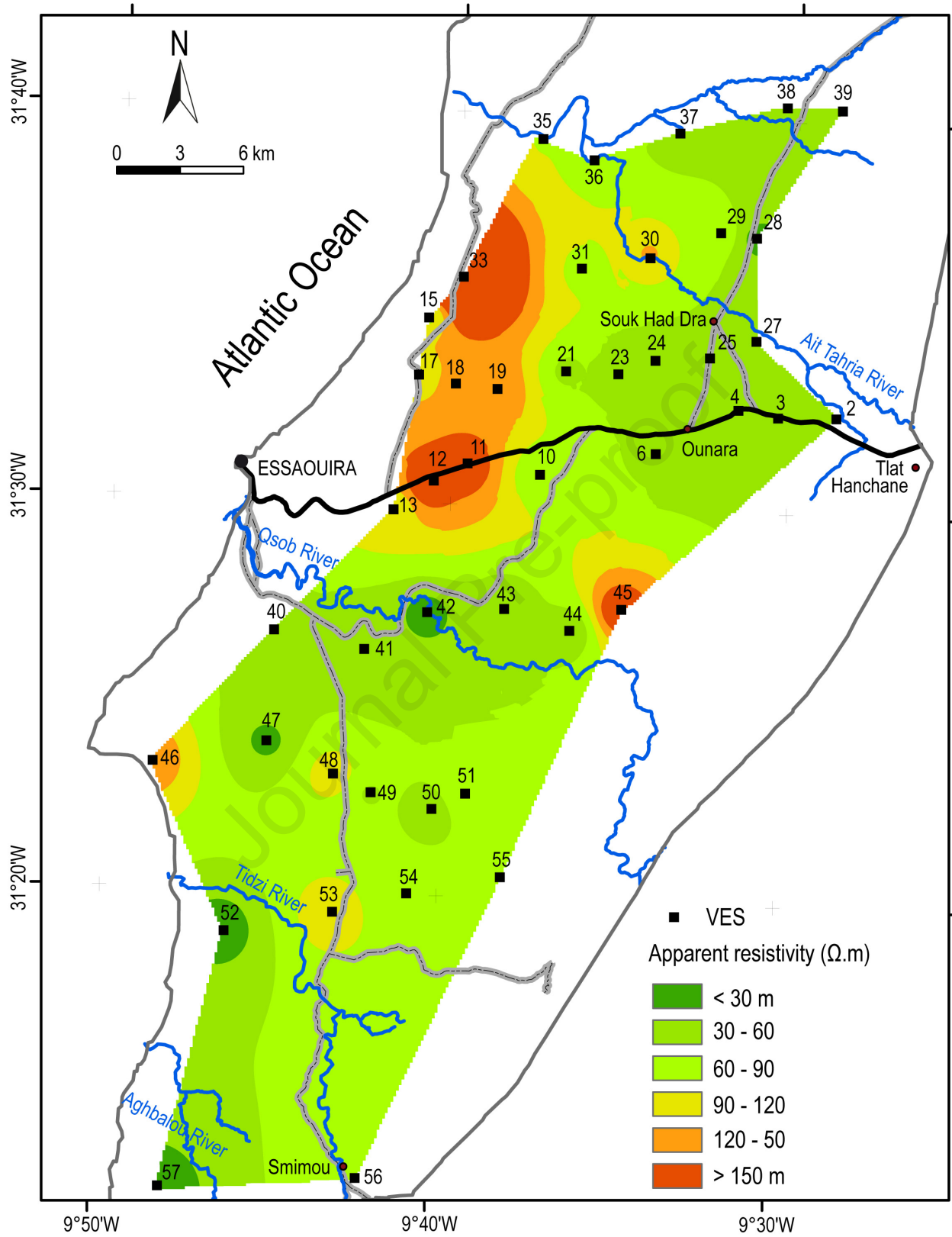


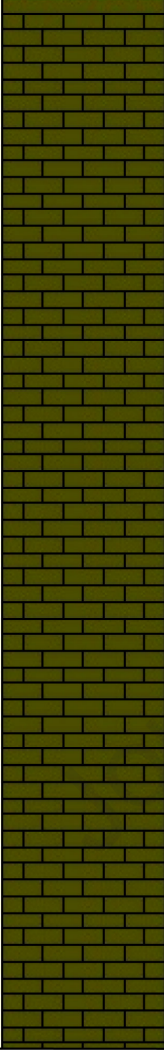


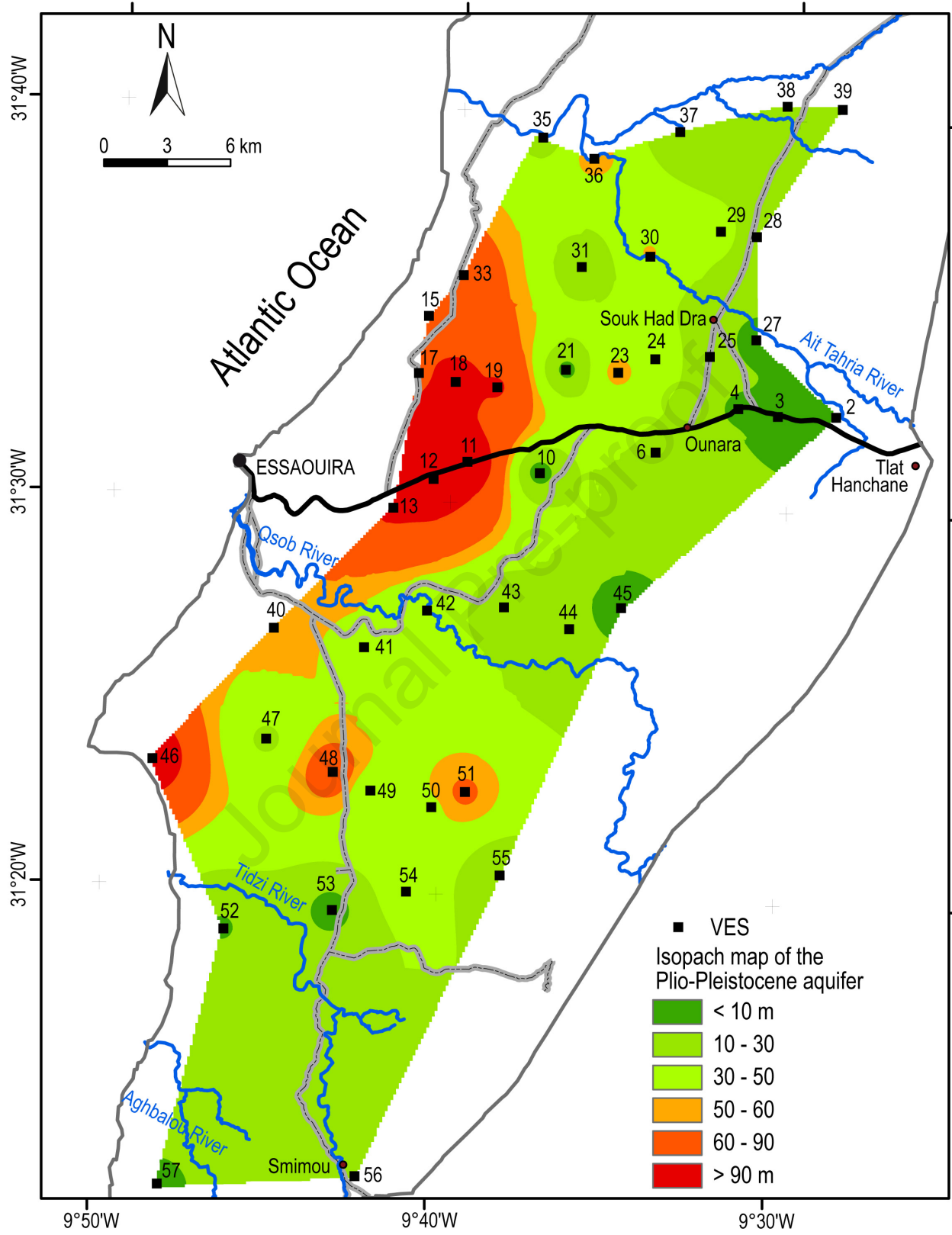


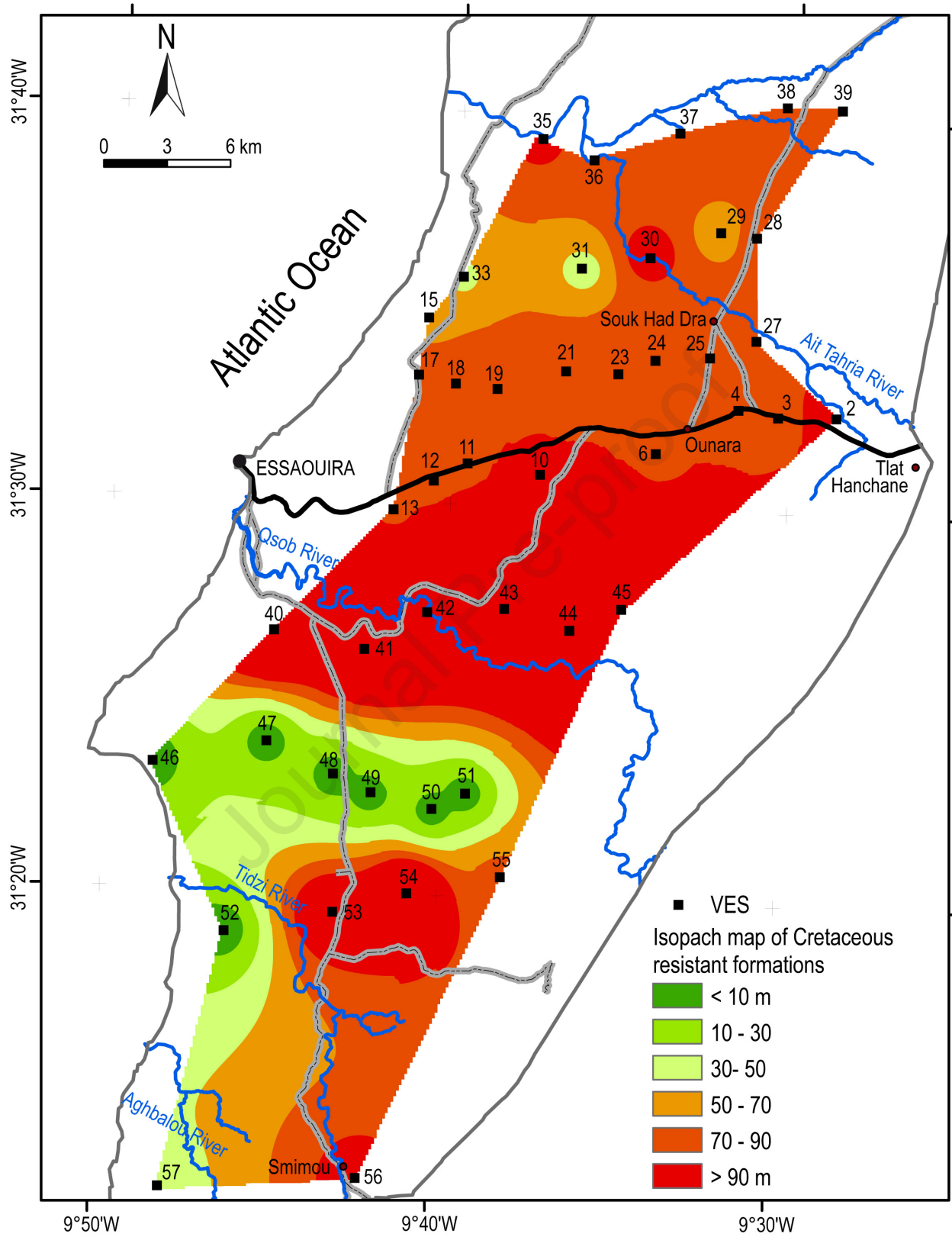


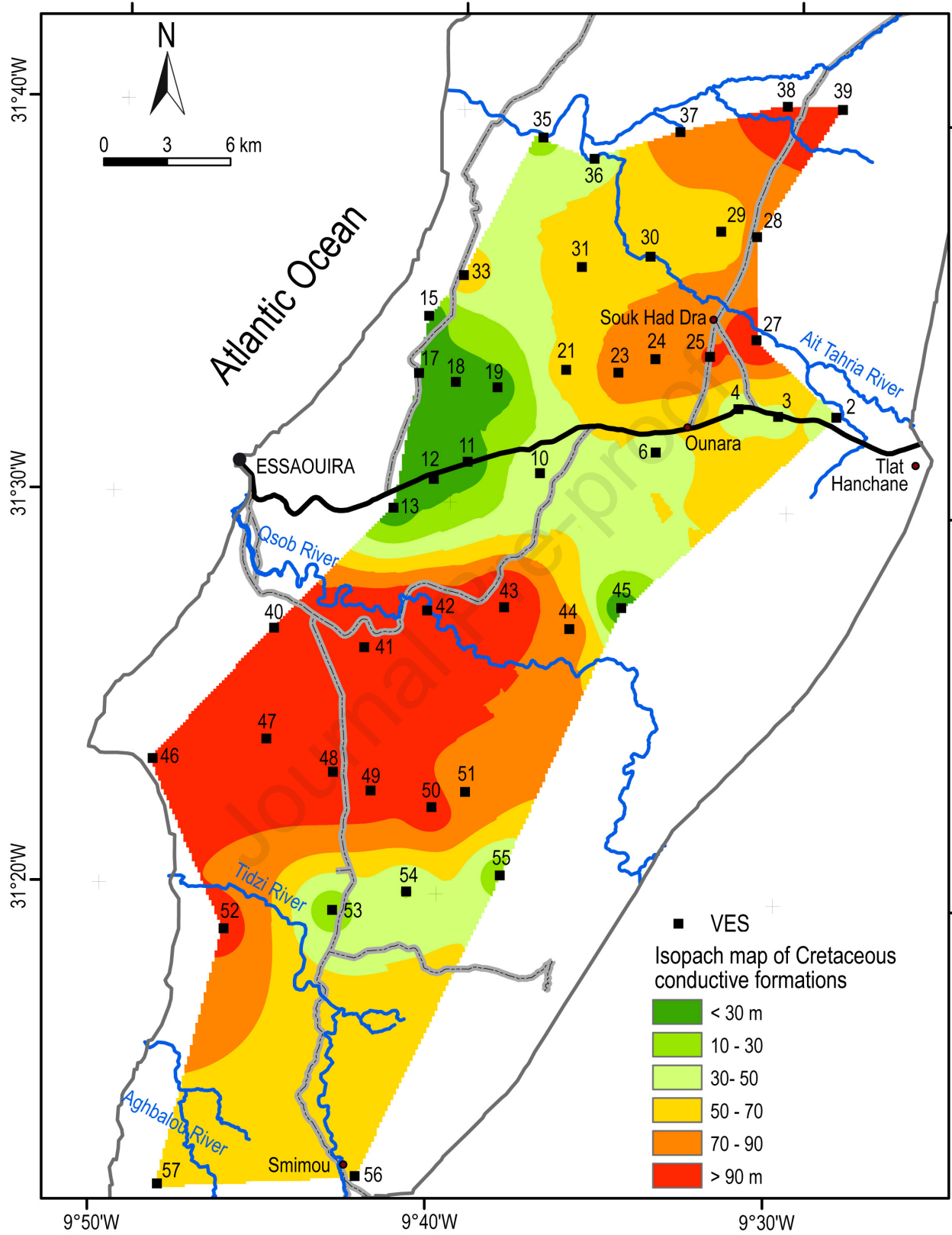


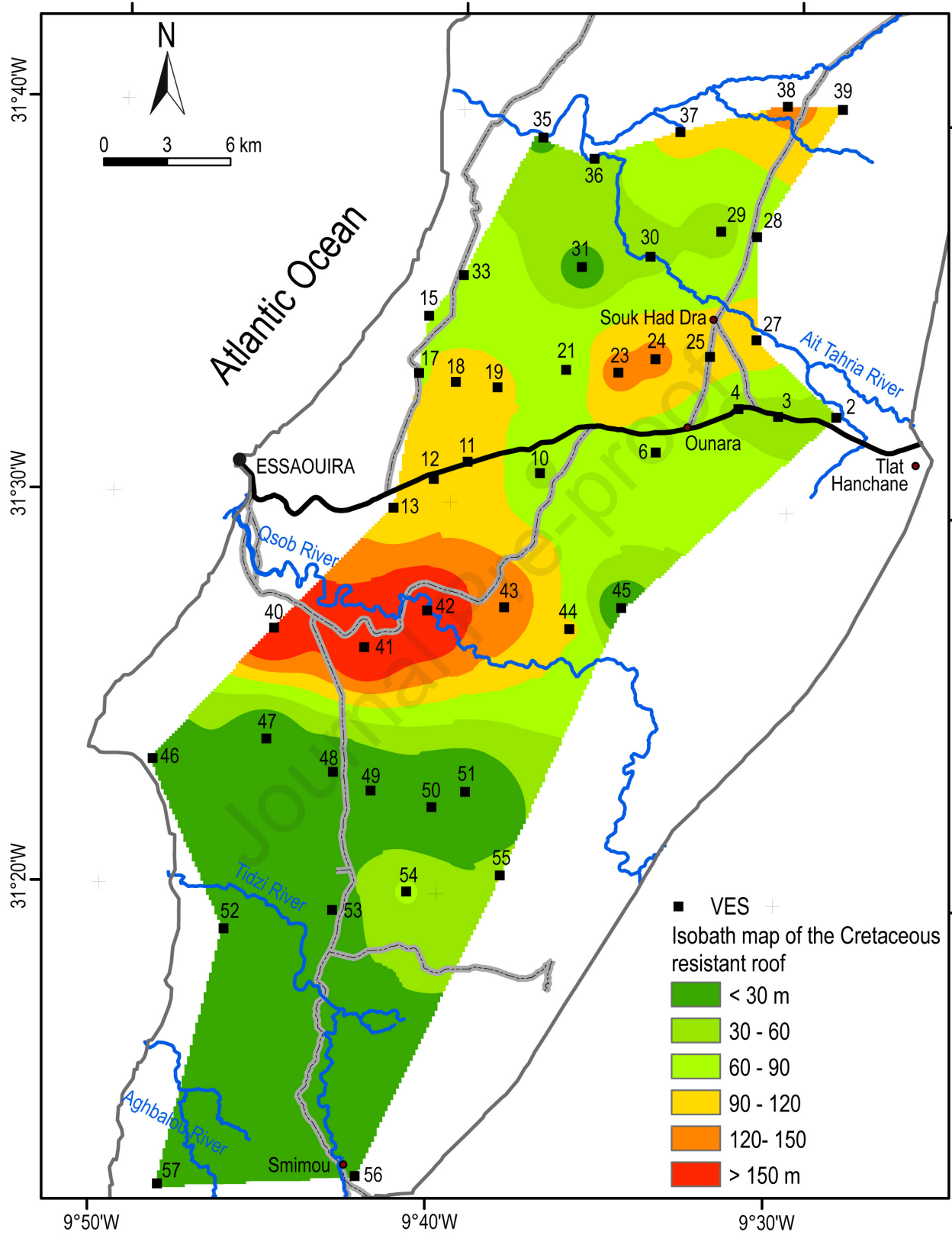


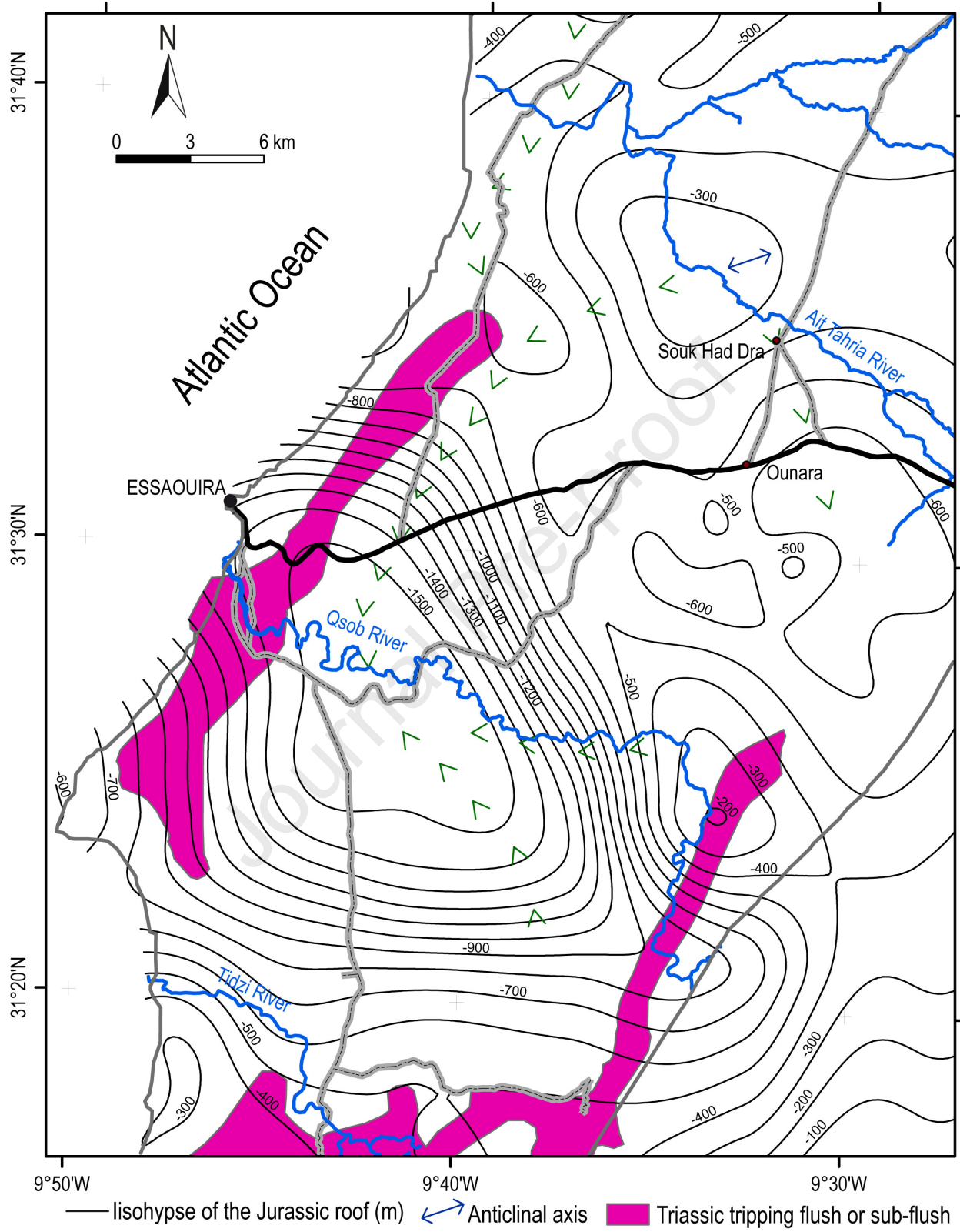
Depth (m)	Lithology	Description	Stage/Age	Resistivity ($\Omega.m$)		
				50	500	950
4		Sandy marls	Plio-Pleistocene			
		Marly limestones	Santonian			
23		Limestones	Tunonian			
152						

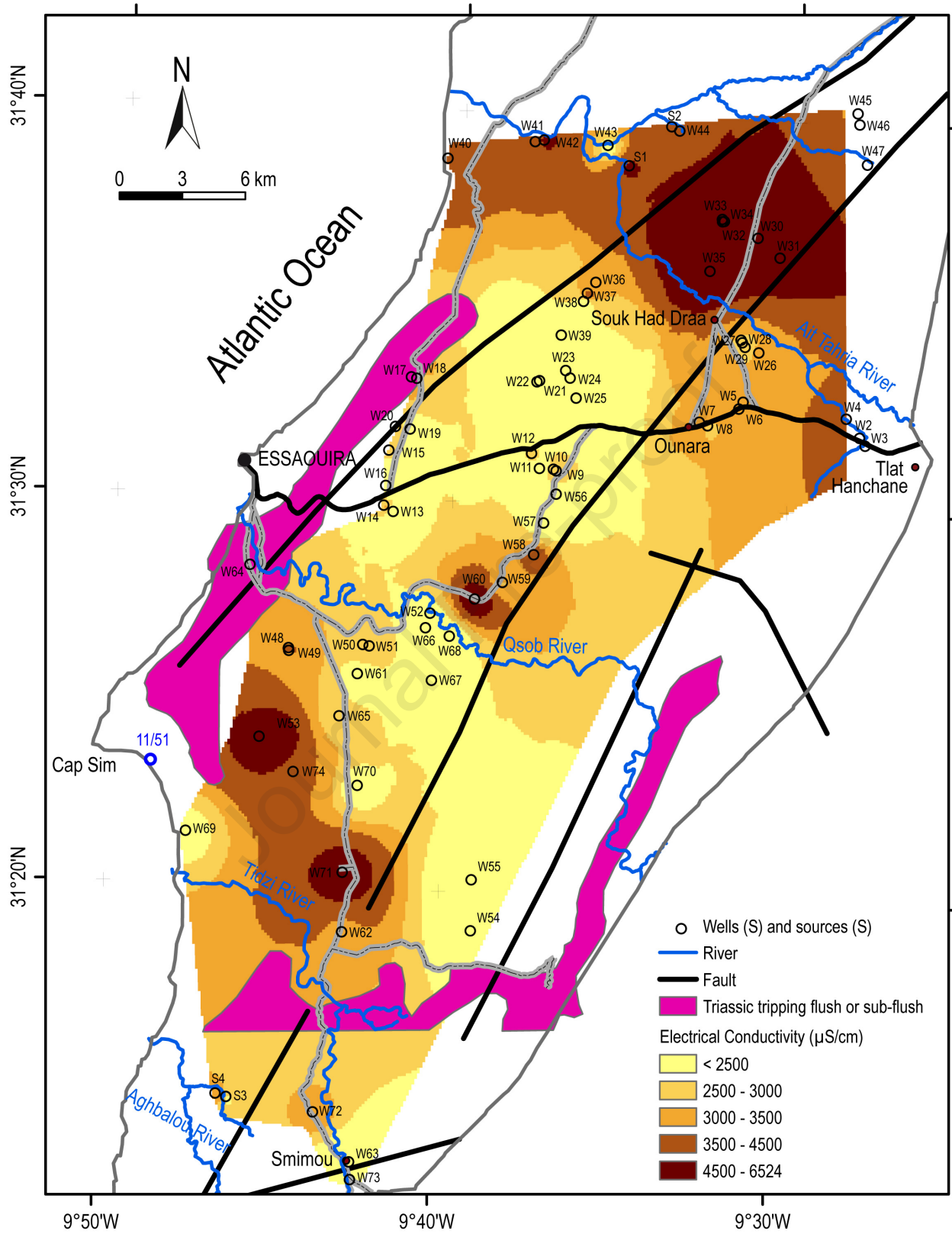












Highlights

- Vertical Electrical Soundings carried out on 45 sites in the Essaouira coastal area, enabled to outline the spatial subsurface distribution of Plio-Pleistocene and Cretaceous aquifers.
- Aquifers exhibit apparent resistivity and thickness values from 44 to 320 Ω .m and from 15 to 56 m, respectively
- Qsob River area shows a thick layer of resistive Plio-Pleistocene and Cretaceous formations
- Isopach and isobath maps of the aquifers confirm their spatial distribution regarding saltwater intrusions
- Major faulting system, NNE-SSW, NNW-SSE and E-W oriented, accommodating small grabens, controls the aquifers

Declaration of interests

The authors declare that they have no known competing financial interests or personal relationships that could have appeared to influence the work reported in this paper.

The authors declare the following financial interests/personal relationships, which may be considered as potential competing interests:

Journal Pre-proof